A post-translational modification of the sheath modulates *Francisella* type VI secretion system assembly and function

Jason Ziveri[1], Cerina Chhuon[2], Anne Jamet[1], Guénolé Prigent[1], Héloïse Rytter[1], Fabiola Tros[1], Monique Barel[1], Mathieu Coureuil[1], Claire Lays[4], Thomas Henry[4], Nicholas H Keep[3], Ida Chiara Guerrera[2]*, Alain Charbit[1]*

[1] Université Paris Descartes, Sorbonne Paris Cité, Bâtiment Leriche, Paris, INSERM U1151 - CNRS UMR 8253, Institut Necker-Enfants Malades. Team 11: Pathogenesis of Systemic Infections, Paris, France

[2] Plateforme protéomique 3P5-Necker, Université Paris Descartes - Structure Fédérative de Recherche Necker, INSERM US24/CNRS UMS3633, Paris 75014, France

[3] Crystallography, Institute for Structural and Molecular Biology, Department of Biological Sciences Birkbeck, University of London, United Kingdom

[4] CIRI, Centre International de Recherche en Infectiologie, Université Lyon, Inserm, U1111, University Claude Bernard Lyon 1, CNRS, UMR5308, École Normale Supérieure de Lyon, Labex Ecofect, Eco-evolutionary dynamics of infectious diseases, F-69007, LYON, France

Running title: IglB phosphorylation and sheath assembly.

Keywords: Type 6 secretion system, Phosphoproteome, *Francisella tularensis*, IglB.

Bâtiment Leriche. 14 Rue Maria Helena Vieira Da Silva CS 61431 - 75993 PARIS – FRANCE

*Corresponding authors: Ida Chiara Guerrera, Alain Charbit.

e-mail: alain.charbit@inserm.fr; chiara.guerrera@inserm.fr

Tel: 33 1 – 72 60 65 11 — Fax: 33 1 - 72 60 65 13

Abstract

Francisella tularensis is a facultative intracellular pathogen that causes the zoonotic disease tularemia in human and animal hosts. This bacterium possesses a non-canonical type VI secretion systems (T6SS) required for phagosomal escape and access to its replicative niche in the cytosol of infected macrophages. KCl stimulation has been previously used to trigger assembly and secretion of the Francisella T6SS in culture. We found that the amounts of essentially all the TSS6 proteins remained unchanged upon KCl stimulation. We therefore hypothesized that a post-translational modification might be involved in T6SS assembly. A whole cell phosphoproteomic analysis allowed us to identify a unique phosphorylation site on IglB, the TssC homologue and key component of the T6SS sheath. Importantly, the phosphorylated form of IglB was not present in the contracted sheath and 3D modeling indicated that the charge repulsion provoked by addition of a phosphogroup on tyrosine 139 was likely to weaken the stability of the sheath structure. Substitutions of the phosphorylatable residue of IglB (tyrosine 139) with alanine or with phosphomimetics prevented T6SS formation and totally impaired phagosomal escape. In contrast, the substitution with the non-phosphorylatable aromatic analog phenylalanine impaired but did not prevent phagosomal escape and cytosolic bacterial multiplication in J774-1 macrophages. Altogether these data suggest that phosphorylation of the sheath participates to T6SS disassembly. Post-translational modifications of the sheath may represent a previously unrecognized mechanism to finely modulate the dynamics of T6SS assembly-disassembly.

Data are available via ProteomeXchange with identifier PXD012507.

Synopsis

Francisella possesses a non-canonical T6SS that is essential for efficient phagosomal escape and access to the cytosol of infected macrophages. KCl stimulation has been previously used to trigger assembly and secretion of the Francisella T6SS in culture. We found that KCl stimulation did not result in an increased production of TSS6 proteins. We therefore hypothesized that a post-translational modification might be involved in T6SS assembly. Using a global and site-specific phosphoproteomic analysis of *Francisella* we identified a unique phosphorylation site on IglB, the TssC homologue and a key component of the T6SS contractile sheath. We show that this site plays a critical role in T6SS biogenesis and propose that phosphorylation may represent a new mechanism affecting the dynamics of sheath formation.

66 ## Introduction

67

68 *Francisella tularensis* is the causative agent of the zoonotic disease tularemia (Luque-
69 Larena, Mougeot et al., 2017, Maurin & Gyuranecz, 2016, Sjostedt, 2007, Sjostedt, 2011).
70 This facultative intracellular pathogen is able to infect a variety of different cell types but, *in*
71 *vivo*, is thought to replicate and disseminate mainly in phagocytes (Santic, Molmeret et al.,
72 2006). Four major subspecies (subsp) of *F. tularensis* are currently listed that all cause a
73 fulminant disease in mice that is similar to tularemia in human (Kingry & Petersen, 2014,
74 McLendon, Apicella et al., 2006). Although the subsp *novicida* (also called *F. novicida) is*
75 rarely pathogenic in human*,* its genome shares a high degree of nucleotide sequence
76 conservation with the human pathogenic species and is thus widely used as a model
77 organism (Brodmann, Dreier et al., 2017, Eshraghi, Kim et al., 2016, Lagrange, Benaoudia et
78 al., 2018).
79 The transcriptional and post-transcriptional regulatory processes, controlling *Francisella*
80 phagosomal escape and cytosolic multiplication, have been already well characterized (Celli
81 & Zahrt, 2013, Charity, Blalock et al., 2009, Cuthbert, Ross et al., 2017, Meibom, Barel et al.,
82 2009, Sjostedt, 2011, Ziveri, Barel et al., 2017). Notably, the crucial role of a 30-kb locus in
83 *Francisella* virulence (**Figure supplement 1**), designated FPI for "Francisella pathogenicity
84 island" (Broms, Sjostedt et al., 2010), has been extensively documented (Clemens, Lee et
85 al., 2018). Of note, the FPI is duplicated three subspecies of *F. tularensis* (subsps *holarctica*,
86 *mediasiatica*, and *tularensis*), but is present in a single copy in *F. novicida* and *F.*
87 *philomiragia*
88 The FPI encodes a Type VI secretion sytem (T6SS) that is essential to promote bacterial
89 phagosomal escape and access to the cytosolic replication niche (Lauriano, Barker et al.,
90 2004, Meyer, Broms et al., 2015, Nano, Zhang et al., 2004). Whereas the transcriptional
91 regulation of the FPI locus has been deeply characterized (Ramsey, Osborne et al., 2015),
92 the molecular mechanisms triggering T6SS assembly and contraction remain largely

93 unknown. Bioinformatic analyses have divided bacterial T6SS in three phylogenetically
94 distinct subtypes (designated T6SSi-iii) (Russell, Wexler et al., 2014). Whereas most of the
95 well-characterized T6SS belong to the T6SSi (including in *P. areruginosa* and *V. cholerae*),
96 *Francisella* is currently the only bacterium to possess a T6SSii (Abby, Cury et al., 2016)
97 known to be exclusively involved in the intracellular life cycle of the pathogen. Phagosomal
98 escape occurs as early as 30 minutes post-infection (Pizarro-Cerda, Charbit et al., 2016).
99 The FPI encodes, in addition to the T6SS components, a number of proteins of unknown
100 functions some of which (such as IglF,PdpC or PdpD) have been proposed to be T6SS
101 effectors (Eshraghi et al., 2016). Very recently, Mougous and co-workers elucidated the
102 function of one substrate of the T6SS (Ledvina, Kelly et al., 2018). This effector (named OpiA
103 for outside pathogenicity island protein A) is a phosphatidylinositol (PI) 3-kinase that acts on
104 the Francisella-containing phagosomal membrane to promote bacterial escape into the
105 cytoplasm.
106 Our current knowledge of the structure and functional assembly of the *Francisella* T6SS are
107 mainly based on recent cryo-electron microscopy data (Clemens, Ge et al., 2015, Nazarov,
108 Schneider et al., 2018) and structural homologies with other members of the T6SSi (Clemens
109 et al., 2015, Nazarov et al., 2018) and references therein). It has been proposed that the
110 tube comprised of IglC subunits (Hcp homologue) that form hexameric rings, fits within the
111 cavity of the IglA/IglB sheath (TssB/C in *Pseudomonas*, VipA/B in *Vibrio*). Contraction of the
112 sheath results in the ejection of the Hcp tube, together with effector proteins located within
113 the tube and on top of the tip of the tube (Vettiger & Basler, 2016). Formation of the
114 contracted *Francisella* T6SS can be mimicked in vitro by high K^+ concentration (Clemens et
115 al., 2015). Yet, the molecular relay for this environmental cue remains uncharacterized.
116 In order to understand the mechanisms underlying this KCl-induced T6SS production, we
117 performed a global proteomic approach on KCl-induced and non-induced bacteria. This
118 analysis revealed that the relative amounts of most FPI proteins were not increased upon
119 KCl stimulation that suggested the possible implication of a post-translational control of T6SS
120 polymerization. We hypothesized that protein phosphorylation might occur in *Francisella* and

121 contribute to the dynamics of T6SS assembly-disassembly. By using state-of-the art mass
122 spectrometry analyses, we indeed identified more than one hundred peptides bearing
123 serine/threonine/or tyrosine phosphorylated residues in the proteome of *F. novicida.* One
124 peptide, corresponding to a phosphorylation of IglB on tyrosine 139 (Tyr139), particularly
125 attracted our attention. IglB is analogous to the TssC protein in canonical T6SS and forms
126 with IglA (TssB homologue) the T6SS contractile sheath (Clemens et al., 2015). The data
127 presented here reveal that phosphorylation of IglB is essential for the proper activity of the
128 T6SS and could contribute to the fine control of T6SS dynamics.

129

130

131 ## Results

132

133 We first monitored sheath formation upon KCl stimulation, using the procedure previously
134 described (Clemens et al., 2015). Briefly, lysates of wild-type *F. novicida,* grown in the
135 presence of 5% KCl, were layered onto 15%-55% sucrose gradients (**Figure 1A**). The
136 fraction sedimenting in equilibrium at 55% sucrose and below (55% Optiprep, grey arrow)
137 from KCl-induced cultures were further dialyzed and used for negative staining TEM imaging.
138 As expected, rod-shaped particles were detected by transmission electron microscopy in this
139 fraction that corresponded to contracted sheath-like structures. The different fractions of the
140 gradient were next tested by western blotting with anti-IglA and anti-IglB antibodies. IglA and
141 IglB were detected in all the fraction of the gradient in KCl-induced conditions (**Figure 1B**). In
142 contrast, they were only detected in the fractions of the upper half of the gradient (in the 15%
143 and in part of the 35% sucrose fractions) in the non KCl-induced conditions. We next decided
144 to perform a whole cell proteome analysis of KCl-induced and non-induced bacterial cultures.

145

146

147

148 **Whole cell proteome analyses**

149 Whole cells extracts from KCl-induced and non-induced cultures were analyzed in order to
150 identify proteins whose intensity was altered by the KCl treatment. We could quantify 1,395
151 proteins that represent 80% of the predicted *Francicella* proteome (**Figure 1C**). Upon KCl
152 stimulation, 113 proteins were up-regulated after KCl stimulation and 97 down-regulated,
153 confirming that KCl stimulation strongly alters the proteome of the cell (**Table supplement**
154 **1**). Remarkably, the amounts of most of the FPI-encoded proteins (17 out the 18 proteins
155 encoded by the FPI were identified) did not change significantly upon KCl stimulation,
156 including notably the sheath and tube proteins IglA, IglB, IglC (blue dots in **Figure 1C**).
157 The down-regulated proteins comprised seven proteins (FTN_0042 to FTN_0048) encoded
158 by the "Francisella novicida island" (or FNI), a genomic island that shows some similarities
159 with the FPI (Rigard, Broms et al., 2016), FTN_0042 and FTN_0043 corresponding to the
160 orthologues of IglA and IglB, respectively). Oppositely, two sets of proteins emerged as up-
161 regulated (**Figure supplement 2A**): proteins involved in Iron-sulfur (Fe/S) clusters
162 biogenesis (FTN_0751 to FTN_0754, FTN_0850 to FTN_0853 and FTN1082) as well as
163 most of the protein encoded by the *fig* (also designated *fsl*) operon (Kiss, Liu et al., 2008,
164 Sullivan, Jeffery et al., 2006), involved in iron acquisition (FTN_1681, FTN_1682, FTN_1684
165 to FTN_1687) (**Figure supplement 2B**). On the basis of the known regulation of Fe/S
166 clusters in other bacterial species (Mettert & Kiley, 2015, Roche, Aussel et al., 2013), these
167 Fe/S cluster proteins could be regulated by FTN_0810, a predicted transcriptional regulator
168 sharing modest sequence identity with the Fe/S regulator IscR.

169

170 **The phosphoproteome of *Francisella***

171 The fact that the amounts of T6SS proteins remained unchanged upon KCl induction, led up
172 to hypothesize that a post-translational mechanism might be responsible for KCl-dependent
173 sheath polymerization. We decided to test if protein phosphorylation could be involved in the
174 process and carried out a global and site-specific phosphoproteomic analysis of *F.*

175 *novicida* (strain U112), based on phosphopeptide enrichment and high-resolution LC-MS/MS
176 analysis of whole cell lysates from KCl-induced and non-induced cultures (**Figure 2**). Overall,
177 this analysis allowed the identification of 103 phosphopeptides, of which 78 were robustly
178 quantified. The majority of the phosphosites (47 out of 78) were found on serine residues (S),
179 while similar lower number of sites, 19 and 12, were found on threonine (T) and tyrosine (Y),
180 respectively (**Figure 2A, B; Tables supplement 1**, **2**). These phosphosites corresponded
181 to 59 proteins, of which 7 presented multiple phosphorylation sites. These proteins belonged
182 to various functional categories and the most represented classes were carbohydrate
183 metabolism, energy production and conversion and translation.
184 IglB was the only protein of the T6SS to be phosphorylated (**Figure 2C**). Furthermore, IglB
185 which constitutes with IglA the T6SS sheath of *Francisella* (Broms et al., 2010, Clemens et
186 al., 2015, Rigard et al., 2016) bore a unique phosphorylation site on Tyr139 (**Table**
187 **supplement 3**). In order to determine if the phosphorylated forms of IglB was incorporated
188 into the sheath upon its assembly, we further analyzed the fractions at the bottom of the
189 gradient (sucrose 55%-Optiprep 55% density zone), containing the sheath-like particles) to
190 the fractions at the top of the gradient (15-35% sucrose density zone, presumably containing
191 non-polymerized forms of the IglA and IglB proteins (hereafter called “heavy fraction”, H or
192 “light fraction”, L, respectively) (**Figure 2D**). The mass spectrometry analysis of the H and L
193 fractions identified over 1,145 proteins (**Table supplement 4**) and confirmed the efficiency of
194 the sucrose gradient separation. Unmodified peptides containing Tyr139 were detected in
195 both H and L fractions, indicating that soluble IglB include both phosphorylated and non-
196 phosphorylated forms of the protein. Importantly, the peptide bearing the phosphorylated
197 tyrosine residue (pY139) of IglB was only detected in the L fraction of the gradient (**Table**
198 **supplement 4**), suggesting that tyrosine phosphorylation might be unfavorable for sheath
199 polymerization.
200 Fully supporting this notion, our 3D predictions (**Figure 3**) indicate that, upon addition of a
201 phosphoryl moiety at this position, charge repulsion between the phosphate group and
202 nearby aspartate residues should be unfavorable for the formation of stable hexameric rings

203 and sheath contraction. Since the phosphate on Y139 is linked to the O^4 position of the
204 phenolic ring, the effects of Tyr phosphorylation may be exerted primarily through
205 allosteric/electrostatic effects. Looking at the full helical reconstruction, one can see that
206 Y139 is close to both D63 of IglA and D114 of IglB. These are from two different symmetry-
207 related chains (**Figure 3**). Putting a phosphate on Y139 is thus likely to repel the aspartate
208 residues and to disassemble the structure.
209

210 **Sequence analyses**

211 Comparative sequence analyses on 33 IglB proteins from 19 genomes of the *Francisella*
212 genus were performed to assess the conservation of residue Tyr139 (**Figure supplement 3**).
213 Sequences were highly conserved between 31 IglB proteins sharing 93 to 100% amino acid
214 identity. In contrast, the proteins encoded by *FTN_0043* in the FNI (Rigard et al., 2016) and
215 *F7308_1917* (Fsp_TX077308) exhibited only 48% amino acid identity with the 31 other IglB
216 proteins whereas they both share 85% identity. Excluding these 2 outliers, among 506 sites,
217 458 were without polymorphism (91%), with Tyr139 conserved in all IglB sequences (**Figure**
218 **supplement 3, upper part**). Since IglB is among the most conserved components of T6SS
219 (Broms et al., 2010, Clemens et al., 2015), we were able to retrieve orthologues of IglB
220 encoded outside of *Francisella* genus. Out of 535 non-redundant IglB orthologues (also
221 named VipB, TssC or EvpB/VC_A0108), we found 90 sequences with a tyrosine in the
222 vicinity of Tyr139 site outside of *Francisella* genus. In 82 sequences, the predicted location of
223 the tyrosine residue was similar to that of Tyr139 (in a turn region between two helices)
224 (**Figure supplement, lower part**).
225

226 We hereafter thoroughly evaluated the importance of Y139 phosphorylation on T6SS
227 functionality and *Francisella* pathogenicity. For this, we constructed two IglB variants in which
228 Tyr139 was substituted either by an alanine (Ala) or by the non-phosphorylatable aromatic
229 amino acid analogue of tyrosine, phenylalanine (Phe). These IglB mutated proteins

230 (designated Y139A and Y139F, respectively) were expressed *in trans* in a Δ*iglB* mutant of *F.*
231 *novicida* carrying a chromosomal deletion of the entire *iglB* gene, (see Materials and
232 Methods). A *F. novicida* mutant with a deletion of the entire *FPI*, unable to escape from
233 phagosomes and hence to grow in macrophages (Weiss, Brotcke et al., 2007), was used as
234 a negative control.
235

236 **A role of IglB phosphorylation in sheath formation**

237 IglB was detected by Western blotting on whole cell lysates in wild-type and complemented
238 mutated strains (Y139A and Y139F) but not in the Δ*iglB* and Δ*FPI* strains (**Figure 4A**). IglA
239 was also detected in wild-type and complemented mutated strains (Y139A and Y139F), but
240 in lower amounts in the Δ*iglB* strain and not in the Δ*FPI* mutant. This observation is in
241 agreement with earlier observations (Broms, Lavander et al., 2009) that suggested that the
242 presence of IglB increases the stability of IglA.
243 A classical measure of basal T6SS function is the export of an Hcp-related protein.
244 Therefore, we examined IglB-dependent IglC export in the different *F. novicida* mutant
245 strains by Western-blot on bacteria grown in the presence -or absence- of 5% KCl. In
246 agreement with previous reports, IglC was detected in the culture supernatant in the
247 presence, but not in the absence, of KCl, in the wild-type and $iglB_{WT}$ complemented strains.
248 In contrast, deletion of *iglB* as well as the two single amino acid substitutions Y139A and
249 Y139F abolished the secretion of IglC into the culture medium (**Figure 4B**). KCl treatment did
250 not modify the amounts of IglA, IglB and IglC proteins detected by western blotting on whole
251 cells (bacterial pellet fractions).
252 To check the impact of the two amino acid substitutions on IglA/IglB heterodimer formation,
253 we performed co-immunoprecipitation assays (**Figure 4C**). We used either anti-IglA to
254 precipitate the complex, followed by western blotting with anti-IglB (upper panel) or anti-IglB,
255 followed by western blotting with anti-IglA (lower panel). In both conditions, the two IglB
256 mutants were still able to interact with IglA to form IglA/IglB heterodimers.

257 We next performed sucrose gradient fractionation (as described above), followed by western
258 blotting with anti-IglB on the Y139F and Y139A mutant strains. The Y139F IglB mutant
259 protein was detected in both the L and H fractions of the gradient (**Figure 4D**), indicating that
260 some sheath polymerization still occurred in the Y139F mutant. In contrast, the Y139A
261 mutant protein was detected in the upper fractions of the gradient but not in the lower
262 fractions (corresponding to the contracted sheath). Fully supporting the western-blot data,
263 proteomic analysis of the distribution of IglA and IglB in the Heavy (H) and light (L) sucrose
264 fraction revealed that their distribution was similar in the strains expressing either WT IglB
265 and Y139F IglB with, in both case, a slightly higher proportion of IglA and IglB in the L
266 fraction compared to the H fraction. In sharp contrast, with the Y139A mutant, IglB was
267 absent from the H fraction and IglA also almost exclusively found in the L fraction (**Figure**
268 **4E).**
269 Altogether, these data comforted the infection assays described above and suggested that
270 the non-phosphorylatable Y139F mutant could still assemble into not fully functional sheath-
271 like structures.
272

273 **Critical role of residue Y139 in *Francisella* pathogenesis**

274 The mutations Y139A and Y139F had no effect on bacterial growth in broth (**Figure**
275 **supplement 4**). The ability of wild-type *F. novicida* (WT), Δ*iglB* and complemented strains
276 (CpWT, Y139A and Y139F) to survive and multiply in murine macrophage-like J774.1 cells
277 was monitored over a 24 h-period (**Figure 5A**). Confirming earlier reports (Spidlova & Stulik,
278 2017), intracellular multiplication of the Δ*iglB* mutant was essentially abolished and
279 comparable to that of the Δ*FPI* mutant. Remarkably, the single amino acid substitution of
280 Tyr139 by Ala (Y139A) also abolished intracellular bacterial multiplication. In contrast, when
281 Tyr139 was substituted by Phe (Y139F), a severe intracellular growth defect was recorded
282 until 10 h after infection (almost fifty-fold less bacterial counts) but at 24 h, the Y139F mutant
283 strain had multiplied and showed only a ten-fold reduction of bacterial counts compared to

284 wild-type, suggesting that a late phagosomal escape had occurred therefore promoting
285 cytosolic bacteria multiplication.
286 As expected, functional complementation (*i.e.,* introduction of a plasmid-born wild-type *iglB*
287 allele into the Δ*iglB* mutant strain (CpWT) restored wild-type growth.
288 We compared the ability of the Δ*iglB* mutants to escape from the phagosomal compartment
289 to that of the wild-type strain by monitoring co-localization of intracellular bacteria with LAMP-
290 1 in J774-1 macrophages (**Figure 5B**), using specific antibodies and automated
291 quantification. The frequency of bacteria co-localizing with LAMP-1 at all 3 time points was
292 elevated (between 60% and 90%), with Δ*iglB* and the two complemented strains expressing
293 mutated *iglB* alleles (designated Y139A and Y139F; respectively). In contrast, co-localization
294 of the wild-type strain with LAMP-1 was below 20% after 1 h and remained in the same
295 range throughout the infection, suggesting that the Δ*iglB* mutant as well as the two strains
296 expressing mutated *iglB* alleles, are still trapped in the phagosomal compartment after 10 h,
297 whereas the wild-type strain has already escaped into the cytosol after 1 h.
298 However, supporting the kinetics data, transmission electron microscopy confirmed that a
299 clear cytosolic multiplication was visible at 24 h with the Y139F mutant but not with the
300 Y139A mutant (**Figure 6A**). We therefore next used time-lapse video microscopy to visualize
301 in real time multiplication of the Y139F mutant in J774-1 macrophages. For this, we inserted
302 a GFP-encoding gene into plasmids pKK214::pGro*iglB* and pKK214::pGro*iglB*Y139F
303 (yielding recombinant plasmids pKK214::pGro*iglB*-pGro*gfp* and pKK214::pGro*iglB*Y139F-
304 pGro*gfp,* respectively). *F. novicida* Δ*iglB* was transformed with these GFP-expressing
305 recombinant plasmids. We generated J774-1 cells with red nuclei by transduction with
306 NucLight Red Lentivirus to facilitate cell recognition and counting (see Materials and
307 Methods). J774-1 cells with red nuclei were infected by GFP-expressing bacteria at an MOI
308 of 1,000. Infection was followed over a 24h-period, using a fully automated microscope
309 Incucyte® 531 S3 (Essen BioScience). Images were taken every 20 minutes with the 20X
310 objective during 24 h, starting 1 h after infection (**Figure 6B** snapshots; **Videos supplement**
311 **1, 2**). Under these conditions, an active intracellular multiplication was observed with both

312 strains. In the conditions used, we observed only a minor delay in bacterial multiplication was
313 observed with the strain complemented with the mutated *iglB* allele Y139F compared to the
314 strain complemented with the wild-type allele, In contrast to the kinetics and LAMP co-
315 localization data that suggested a retarded phagosomal escape of the Y139F mutant. Hence,
316 it is likely that the Y139F substitution allows the production of sufficient assembled T6SS to
317 promote bacterial phagosomal escape and cytosolic multiplication in these cells.
318
319 Finally, we replaced Tyr139 by two phosphomimetics *i.e.* the negatively charged amino acids
320 Aspartate and Glutamate and evaluated the impact of these amino acid substitutions (Y139D
321 and Y139E) on intracellular multiplication in J774-1 cells (**Figure supplement 6A**). The two
322 mutants led to severe defects in intracellular multiplication and, at all time points tested, the
323 replication defect was comparable to that of the Y139A or Δ*FPI* mutant. We next evaluated
324 the capacity of the Y139D and Y139E mutants to form sheath-like structure by using the
325 sucrose gradient assay. In the two mutants, the IglB protein was exclusively detected by
326 Western blot in the upper fractions of the sucrose gradient (**Figure supplement 6B**). These
327 data strongly suggest that residues possibly mimicking the phosphorylated state of Y139 also
328 prevented sheath-like assembly.
329
330 Of note, in primary bone marrow-derived macrophages (BMMs), growth of the Δ*iglB* deletion
331 mutant as well as that of the two Y139A or Y139F was similar to that of a Δ*FPI* mutant
332 (**Figure supplement 5A**) at all time points tested. Functional complementation restored
333 normal intracellular bacterial replication (in CpWT). The ability of the Δ*iglB* mutants to induce
334 phagosomal membrane rupture in BMMs was further tested by using a CCF4 assay,
335 essentially as previously described (Ramond, Gesbert et al., 2015, Rigard et al., 2016). Wild-
336 type *F. novicida* and CpWT strains showed similar amount of cleaved CCF4 at the three
337 time-points tested (1 h, 3 h and 6 h) whereas there was no (or marginal) loss of FRET signal
338 with Δ*iglB* (**Figure supplement 5B**), Y139A, Y139F, and the two negative control strains
339 (Δ*FPI* and Δ*bla*), indicating that the Y139A, Y139F mutant strains remained stuck in intact

340 phagosomes during the time-period tested in BMMS. Hence in primary macrophages, a
341 tyrosine residue is required for an optimal T6SS assembly likely due to their high bactericidal
342 activity. Moreover, in the mouse model of tularemia (see Materials and Methods for details),
343 the two mutants Y139A and Y139F also showed an almost complete loss of virulence (**Fig**
344 **S5C)** that confirmed the critical role of tyrosine residue 139 of IglB in Francisella
345 pathogenicity.
346

347 **Searching for putative kinases**

348 Our careful inspection of the *Francisella* genomes did not identify any gene encoding for a
349 putative serine/threonine- or tyrosine-kinase. We therefore searched for proteins containing
350 potential tyrosine kinase domains. Using the PFAM database (https://pfam.xfam.org/), we
351 could identify three candidates proteins (FTN_1082, FTN_0459 and FTN_1433). FTN_1082
352 is predicted to belong to the uncharacterized ACR,YdiU motif/UPF0061 family (PFAM
353 database PF02696). This protein family notably comprises the SELO proteins (for
354 selenoproteins) that have been proposed to constitute a novel ubiquitous kinase-like family of
355 proteins. Recent bioinformatic analyses have identified FTN_1082 as a potential SELO
356 family-member (Dudkiewicz, Szczepinska et al., 2012). FTN_0459, is predicted to encode a
357 UbiB homologue, The UbiB protein family is also a widespread family of kinase-like present
358 in the three kingdoms of life, often required for the biosynthesis of isoprenoid lipids. In
359 *Escherichia coli,* UbiB has been shown to be required for the aerobic biosynthesis of the
360 redox-active lipid ubiquinone, coenzyme Q (Aussel, Pierrel et al., 2014). It has been
361 assumed but not formally established that UbiB family members were protein kinases.
362 However, very recently it was demonstrated that a UbiB family member, the mitochondrial
363 protein ADCK3, adopted a PKL fold and bound adenine nucleotides in a divalent cation-
364 dependent manner strongly supporting the hypothesis that UbiB proteins are bona fide
365 kinases (Stefely & Pagliarini, 2017). Finally, FTN_1433, is a protein bearing a G-rich domain
366 identified on putative tyrosine kinase (PFAM database PF02706). This family notably
367 includes proteins involved in lipopolysaccaride biosynthesis (Wzz proteins).

368 We anticipated that if one of these genes was involved in IglB phosphorylation, its
369 inactivation would impair phagosomal escape and hence cytosolic bacterial multiplication.
370 We therefore monitored intracellular bacterial multiplication of the three corresponding
371 transposon insertion mutants of *F. novicida* (Gallagher, Ramage et al., 2007) after 10 hours
372 in J774-1 macrophages (**Figure supplement 7**). The three mutants showed wild-type
373 intracellular multiplication in this assay, suggesting that either these proteins work
374 synergistically or that there exists another yet unidentified enzyme with a moonlight tyrosine
375 kinase activity.
376
377

378 Discussion

379
380 We show here that the unique phosphorylated residue of the sheath component IglB plays a
381 critical role in T6SS functional assembly, bacterial phagosomal escape and virulence. This
382 post-translational modification of IglB might contributes to the fine tuning of T6SS
383 disassembly.
384

385 Pivotal role of residue 139 in sheath assembly

386 The assembly of the T6SS-H1 of *Pseudomonas aeruginosa* has been shown to be spatially
387 regulated by a post-translational mechanism coined « the Threonine Protein
388 Phosphorylation » (or TPP) Pathway. During this process, involved in the defense of bacteria
389 to a neighboring attack, a membrane-bound threonine kinase phosphorylates a forkhead-
390 associated domain-containing Protein (FhA or TagH), which promotes the assembly of an
391 active conformation of the T6SS at the site of the attack (Cianfanelli, Monlezun et al., 2016,
392 Mougous, Gifford et al., 2007). More recently, the offensive anti-bacterial T6SS of *Serratia*
393 *marcescens* has also been shown be controlled by the opposing actions of the TPP pathway
394 and TagF on assembly of the core machinery (Ostrowski, Cianfanelli et al., 2018). The TPP

395 represents the only currently identified post-translational mechanism regulating T6SS
396 biogenesis.
397 In bacteria such as *Escherichia coli, Vibrio cholerae* or *Pseudomonas aeruginosa*, the sheath
398 contracts spontaneously during the repeated rounds of ultraspeed purification required for
399 their isolation from cell cultures (Nguyen, Douzi et al., 2018). In *Francisella*, T6SS contraction
400 can be triggered in culture either by placement under coverslips or by KCl stimultation
401 (Clemens et al., 2015). Our mass spectrometry analyses revealed that T6SS proteins were
402 not upregulated upon KCl treatment and that IglB was the only T6SS protein to contain a
403 phosphorylated residue (Tyr139). Importantly, the phosphorylated form of IglB was not
404 associated with the contracted sheath (**Figure 2**) that suggested that the phosphorylation
405 status of IglB residue Tyr139 could participate to T6SS dissociation.
406 Formation of the *Francisella* T6SS is believed to occur in the phagosome before cytosolic
407 escape of the bacterium and the T6SS seems to be dispensable for cytosolic multiplication.
408 Nevertheless, some T6SS elements are likely to be required during the cytosolic stage of the
409 infectious cycle. Indeed, most FPI genes are induced during late intra-macrophage growth
410 (Wehrly, Chong et al., 2009) and IglC has been shown to be required for intracellular growth
411 of *F. novicida* that are microinjected directly into the cytosol of HeLa cells (Meyer et al.,
412 2015). IglC secretion in *F. novicida* depends on the T6SS core components IglA and IglB
413 (Ludu, de Bruin et al., 2008). Of note, truncated IglA proteins still able to form IglA/IglB-
414 heterodimers have been reported to have lost their IglC secretory function (Clemens et al.,
415 2015) that suggests that heterodimer formation is not sufficient to generate a functional
416 sheath.
417 The drastic impact of both Y139A and Y139F substitutions on bacterial virulence (**Figure**
418 **supplement 5**) demonstrated that tyrosine residue 139 of IglB plays a critical role in the
419 functional assembly of the T6SS. Remarkably, the Y139F mutant, which corresponds to the
420 substitution of a tyrosine residue by its non-phosphorylatable aromatic analog phenylalanine,
421 could still assemble unstable sheath-like structure (**Figure 4D, E**) and multiply in J774-1
422 macrophages (**Figure 5A; Figure 6A, B; video supplement 2**) and. At this stage, the

423 inability of the Y139F mutant to form stable T6SS might be explained by the fact that it lacks
424 the OH moiety on the C4 of the phenol ring. Indeed, several reports support the notion that
425 the OH moiety of tyrosine residues may participate to protein functionality and stability. For
426 example it has been shown that intramolecular hydrogen may contribute significantly to
427 conformational protein stability (Bolen & Rose, 2008). Since the OH moiety is capable of
428 forming such intra- or intermolecular hydrogen bonds with the carboxy oxygen of adjacent
429 amino acid residues, when a Tyr-Phe substitution is made in a protein, it is likely to impact its
430 folding or stability (Pace, Horn et al., 2001). More recently, (Baroni, Pandini et al., 2012) also
431 demontrated that a single tyrosine Hydroxyl Group controled the specificity of *Plasmodium*
432 *falciparum* ferredoxin-NADP+ reductase. Although inspection of the 3.7 Å EM reconstruction
433 of the *F. novicida* contracted sheath (PDB 3j9o) does not show any atoms close enough to
434 form a hydrogen bond with the hydroxyl of Tyr139, the carboxylates of Asp114 from IglB, and
435 Asp63 of IglA in the next dimer, are around 5 Å away and these may approach close enough
436 to Tyr139 OH to form hydrogen bond interactions stabilizing the assembly.
437 3D modeling also indicated that there is space for a phosphate group on this atom as the OH
438 is pointing into a pocket in the structure (**Figure 3**). However, the negatively charged
439 phosphate would induce charge repulsion with the nearby Asps from the next dimer most
440 likely preventing assembly of the strands when Tyr139 is phosphorylated. Hence, the charge
441 repulsion provoked by addition of the phosphogroup (when Y139 is phosphorylated) is likely
442 to weaken the stability of the contracted sheath. Altogether these data suggest that the
443 phosphorylation status of IglB could modulate T6SS assembly/disassembly process.
444 Supporting the notion that phosphorylation of Tyr139 impairs sheath contraction,
445 replacement of this residue by a phosphomimetic (Y139D or Y139E) led to a severe
446 intracellular multiplication defect and prevented sheath-like structure formation.
447

448 **IglB phosphorylation, a new partner of T6SS dissociation**

449 Basler and co-workers have recently shown that *F. novicida* assembled its T6SS sheath on
450 the bacterial poles (Brodmann et al., 2017) and that the sheath cycled through assembly,

451 contraction and disassembly, similarly to what was previously described for other canonical
452 T6SSs. The FPI does not encode any homologue of the unfoldase ClpV, present in all the
453 canonical T6SS, but instead uses the general chaperone ClpB for the recycling of the
454 contracted sheaths (Brodmann et al., 2017). ClpB specifically localizes with the contracted
455 sheaths and is responsible for their disassembly within phagosomes of infected
456 macrophages. We found that the amounts of ClpB were not (or marginally) up-regulated
457 upon KCl induction (*i.e.* only 1.3-fold more ClpB in KCl-induced conditions compared to non-
458 induced conditions). ClpB was also mainly associated with the soluble fraction of the sucrose
459 gradient of KCl-induced bacteria (**Table supplement 1**). The kinase activity, leading to IglB
460 phosphorylation might assemble, like ClpB, at the pole of the bacterium only when the
461 sheath is contracted and assist sheath dissociation.
462 In spite of our repeated attempts, we were unable to identify a candidate tyrosine kinase.
463 This suggests that a yet unidentified enzyme with either a non-canonical tyrosine kinase
464 activity or a protein predicted to be involved in a different enzymatic reaction with a
465 « moonlight » tyrosine kinase activity, is responsible for IglB phosphorylation. If so, its
466 identification might prove extremely difficult and would require extensive future work. It is
467 also possible that a single kinase mutant might have no or very limited effect on phagosomal
468 disruption since sheath polymerization would occur and be sufficient to promote phagosomal
469 membrane disruption. Indeed, it has been shown (Meyer et al., 2015) that only a minor
470 fraction of functional T6SS is sufficient to promote phagosomal escape and, once in the
471 cytosol, FPI mutants can multiply like wild-type bacteria.
472 Our whole cell proteomic analysis revealed that the amounts of more than two hundred
473 proteins were altered upon KCl stimulation (**Figure 1**). Notably, the down-regulated proteins
474 comprized seven proteins (FTN_0042 - FTN_0048) out of the 13 proteins potentially
475 encoded by the *Francisella novicida* island (FNI, FTN_0042 - FTN_0054) (Rigard et al.,
476 2016). Although inactivation of the whole FNI locus had no effect on *F. novivcida* virulence
477 (Rigard et al., 2016), a possible contribution of the orthologues of IglA and IglB (FTN_0042
478 and FTN_0043) to the sheath assembly-disassembly process cannot be excluded. The

479 proteins involved in Iron-sulfur (Fe/S) clusters biogenesis or in iron acquisition, that were
480 upregulated upon KCL stimulation might also contribute to T6SS biogenesis.
481 In conclusion, we have identified in the present work a critical residue of IglB whose
482 phosphorylation may represent a new player involved in the fine-tuning of the T6SS
483 dynamics of *Francisella*. Such post-translational sheath modifications might exist in other
484 bacteria that need to be explored.
485
486
487
488
489

490 ## Materials and Methods

491

492 **Ethics Statement**. All experimental procedures involving animals were conducted in
493 accordance with guidelines established by the French and European regulations for the care
494 and use of laboratory animals (Decree 87–848, 2001–464, 2001–486 and 2001–131 and
495 European Directive 2010/63/UE) and approved by the INSERM Ethics Committee
496 (Authorization Number: 75-906).

497

498 ### Strains and culture conditions

499 All strains used in this study are derived from *F. tularensis* subsp. *novicida* U112 (*F. novicida*)
500 as described in **Table supplement 5**. Strains were grown at 37°C on pre-made chocolate
501 agar PolyViteX plates (BioMerieux), Schaedler K3 or Chemically Defined Medium (CDM).
502 The CDM used for *F. novicida* corresponds to standard CDM (Chamberlain, 1965) without
503 threonine and valine (Gesbert, Ramond et al., 2014). For growth condition determination,
504 bacterial strains were inoculated in the appropriate medium at an initial OD_{600} of 0.05 from an
505 overnight culture in Schaedler K3 medium.

506

507 ### Construction of a Δ*iglB* deletion mutant

508 We inactivated the gene *iglB* in *F. novicida* (*FTN_1323*) by allelic replacement, resulting in
509 the deletion of the entire gene (4 first codons and 7 last codons were conserved). We
510 constructed a recombinant PCR product containing the upstream region of the gene *iglB*
511 (*iglB*-UP), a kanamycin resistance cassette (*nptII* gene fused with *pGro* promoter) and the
512 downstream region of the gene *iglB* (*iglB*-DN) by overlap PCR. Primers *iglB* upstream FW
513 (p1) and *iglB* upstream (spl_K7) RV (p2) amplified the 689 bp region upstream of position +3
514 of the *iglB* coding sequence (*iglB*-UP), primers *pGro* FW (p3) and *nptII* RV (p4) amplified the
515 1091 bp kanamycin resistance cassette (*nptII* gene fused with *pGro* promoter); and primers
516 *iglB* downstream (spl_K7) FW (p5) and *iglB* downstream RV (p6) amplified the 622 bp region

517 downstream of the position +1520 of the *iglB* gene coding sequence (*iglB*-DN). Primers p2
518 and p5 have an overlapping sequence of 12 nucleotides with primers p3 and p4 respectively
519 resulting in fusion of *iglB*-UP and *iglB*-DN with the cassette after cross-over PCR (**Table S6**).
520 All single fragment PCR reactions were realized using Phusion High-Fidelity DNA
521 Polymerase (ThermoScientific) and PCR products were purified using NucleoSpin® Gel and
522 PCR Clean-up kit (Macherey-Nagel). Overlap PCRs were carried out using 100 ng of each
523 purified PCR products and the resulting fragment of interest was purified from agarose gel.
524 This fragment was then directly used to transform wild type *F. novicida* by chemical
525 transformation (Gesbert, Ramond et al., 2015). Recombinant bacteria were isolated on
526 Chocolate agar plates containing kanamycin (10 µg mL^{-1}). The mutant strains were checked
527 for loss of the wild type gene by PCR product direct sequencing (GATC-biotech) using
528 appropriate primers.
529

530 **Functional complementation**

531 The Δ*iglB* mutant strain was transformed with the recombinant pKK214-derived plasmids
532 (pKK-*iglBY139A*$_{cp}$, pKK-*iglBY139F*$_{cp}$, pKK-*iglBY139D*$_{cp}$ and pKK-*iglBY139E*$_{cp}$) described
533 below (**Table supplement 5**). Primers pGroFW and pGro RV amplified the 328 bp of the
534 *pGro* promoter; primers *iglB* FW/ and *iglB*[PstI] RV amplified the 1,534 bp *iglB* gene from
535 U112. PCR products were purified and SmaI (*pGro* promoter) or PstI (*iglB*) digested in
536 presence of FastAP Thermosensitive Alkaline Phosphatase (ThermoScientific) to avoid self-
537 ligation. Mixtures of *pGro* promoter and fragments of the genes of interest were then
538 incubated with T4 DNA Ligase (New England Biolabs) to allow blunt end ligation and
539 fragments were then cloned in pKK214 vector after SmaI/PstI double digest and transformed
540 in *E. coli* TOP10. Recombinant plasmid pKK-*iglB*$_{cp}$ was purified and directly used for
541 chemical transformation in *F. novicida* Δ*iglB* (Gesbert et al., 2015). Recombinant colonies
542 were selected on Chocolate agar plates containing tetracycline (5 µg mL^{-1}) and kanamycin
543 (10 µg mL^{-1}).

544 For site-directed mutagenesis of *iglB* gene, we used plasmid pKK-*iglB*$_{cp.}$ The recombinant
545 plasmids pKK-*iglBY139A*$_{cp}$, pKK-*iglBY139F*$_{cp}$, pKK-*iglBY139D*$_{cp}$ and pKK-*iglBY139E*$_{cp}$ were
546 constructed using the primer pairs iglB (Y/A, Y/F,Y/D, or Y/E) FW and iglB RV (**Table**
547 **supplement 6**). The three first bases of primers iglB FW were modified to change Tyr139 to
548 Ala, Phe, Asp or Glu
549 PCR products were purified, phosphorylated by the T4 Polynucleotide Kinase and then
550 incubated with T4 DNA Ligase (New England Biolabs) and transformed in *E. coli* TOP10.
551 Recombinant plasmids were purified and directly used for chemical transformation in *F.*
552 *novicida* Δ*iglB*, as described previously (Gesbert et al., 2015). Recombinant colonies were
553 selected on Chocolate agar plates containing tetracycline (5 µg mL^{-1}) and kanamycin (10 µg
554 mL^{-1}).
555

556 **Gfp-expressing *F. novicida***

557 The Δ*iglB* mutant strain was transformed with the recombinant plasmids pKK-GFP-*iglBWT*$_{cp}$
558 and pKK-GFP-*iglBY139F*$_{cp,}$ derived from pKK214-GFP (Abd, Johansson et al., 2003).
559 Primers pGro (KlionskyAbdelmohsen et al.)FW and *iglB*(Klionsky et al.) RV (**Table**
560 **supplement 5**) amplified the 1,870 bp of the *pGro-iglB* from the pKK-*iglBWT*$_{cp}$ and pKK-
561 *iglBY139F*$_{cp}$. PCR products were purified and digested with SmaI and the *pGro-iglB WT* and
562 *pGro-iglB Y139F* fragments were then incubated with T4 DNA Ligase (New England Biolabs)
563 to allow blunt end ligation and fragments were then cloned in the unique SmaI site of
564 pKK214-(GFP) vector and transformed in *E. coli* TOP10. Recombinant plasmid pKK-(GFP)-
565 *iglBWT*$_{cp}$ and pKK-(GFP)-*iglBY139F*$_{cp}$ were purified and directly used for chemical
566 transformation in *F. novicida* Δ*iglB* (Gesbert et al., 2015). Recombinant colonies were
567 selected on Chocolate agar plates containing tetracycline (5 µg mL^{-1}) and kanamycin (10 µg
568 mL^{-1}).
569
570

571 **Immunodetection**

572 Antibodies to IglA, IglB and IglC were obtained through the NIH Biodefense and Emerging
573 Infections (BEI) Research Resources Repository, NIAID, NIH.

574 ***Immunoblotting analysis.*** Protein lysates for immunoblotting were prepared by using
575 Laemmli sample buffer. Protein lysates corresponding to equal OD_{600} were loaded on 12%
576 Bis/Tris gels (Invitrogen), and run in TGS buffer. Primary antibodies (anti-IglA or anti-IglB)
577 were used at final dilution of 1:2,000. Secondary horseradish peroxidase (HRP)-conjugated
578 goat anti-mouse antibody (Santa Cruz Biotechnology, CA, USA) or (HRP)-conjugated goat
579 anti-rabbit antibody and the enhanced Chemiluminescence system (ECL) (Amersham
580 Biosciences, Uppsala, Sweden) were used as previously described (Ziveri, Tros et al., 2017).

581 ***Co-immunoprecipitations.*** Wild-type *F. novicida* was grown to late exponential phase in
582 Schaedler K3; collected by centrifugation and lysed with lysozyme and 1% TritonX-100
583 detergent in 20 mM Tris HCl, (pH 7.8) with 1 mM EDTA, protease inhibitor cocktail and
584 benzonase nuclease. The lysate was centrifuged at 15,000 g for 15 min at 4°C to pellet
585 bacterial debris. Monoclonal anti-IglB antibody was incubated 40 min with Dynabeads protein
586 G (Invitrogen) and the complex was incubated at room temperature with the bacterial lysate
587 for 1 hour. After washing, the complex was loaded on 12% Bis/Tris gels (Invitrogen), and run
588 in TGS buffer.

589

590 **T6SS purification**

591 T6SS were prepared essentially as described in (Clemens et al., 2015). Briefly, wild-type *F.*
592 *novicida* was grown to late exponential phase in Schaedler K3 containing 5% KCl; pelleted
593 by centrifugation and lysed with lysozyme and 1% TritonX-100 detergent in 20 mM Tris HCl,
594 (pH 7.8) with 1 mM EDTA, protease inhibitor cocktail and benzonase nuclease. The lysate
595 was centrifuged 3 times at 15,000 g for 30 min at 4°C to pellet bacterial debris, and the
596 supernatant was layered onto a 10%–55% sucrose gradient overlying a 55% Optiprep
597 cushion and centrifuged at 100,000 g for 18 hr. Fractions were collected and examined by
598 TEM negative staining using 2% uranyl acetate. The sheath-like structures sedimented to

599 just below the 55% sucrose/Optiprep interface.

600

601 **Phosphoproteomic analyses**

602 ***Reagents and chemicals.*** For protein digestion, dithiothreitol, iodoacetamide and
603 ammonium bicarbonate were purchased from Sigma-Aldrich (St Louis, MO, USA). For
604 phosphopeptide enrichment and LC-MS/MS analysis, trifluoroacetic acid (TFA), formic acid,
605 acetonitrile and HPLC-grade water were purchased from Fisher Scientific (Pittsburgh, PA,
606 USA) at the highest purity grade.

607 ***Protein digestion.*** For proteomic analysis, *F. novicida* was analysed in three independent
608 biological replicates. Protein concentration was determined by DC assay (Biorad, CA, USA)
609 according to the manufacturer's instructions. An estimated 1.2 mg of proteins for each
610 biological replicates were digested following a FASP protocol (Lipecka, Chhuon et al., 2016)
611 slightly modified. Briefly, proteins were reduced using 100 mM dithiothreitol in 50 mM
612 ammonium bicarbonate for 1h at 60°C. Proteins were then split into four samples of 300 µg
613 and applied on 30 kDa MWCO centrifugal filter units (Microcon, Millipore, Germany, Cat No
614 MRCF0R030). Samples were mixed with 200 µL of 8M urea in 50 mM ammonium
615 bicarbonate (UA buffer) and centrifuged for 20 min at 15,000 x g. Filters were washed with
616 200 µL of UA buffer. Proteins were alkylated for 30min by incubation in the dark at room
617 temperature with 100 µL of 50 mM iodoacetamide in UA buffer. Filters were then washed
618 twice with 100 µL of UA buffer (15,000 x g for 15 min) followed by two washes with 100 µL of
619 50 mM ammonium bicarbonate (15,000 x g for 10 min). Finally, sequencing grade modified
620 trypsin (Promega, WI, USA) was added to digest the proteins in 1:50 ratio for 16 h at 37°C.
621 Peptides were collected by centrifugation at 15,000 x g for 10min followed by one wash with
622 50mM ammonium bicarbonate and vacuum dried.

623 ***Phosphopeptides enrichment by titanium dioxide (TiO_2) and phosphopeptides***
624 ***purification by graphite carbon (GC).*** Phosphopeptide enrichment was carried out using a
625 Titansphere TiO_2 Spin tip (3 mg/200 µL, Titansphere PHOS-TiO, GL Sciences Inc, Japan) an
626 estimated 1.2 mg of digested proteins for each biological replicate. Briefly, the TiO_2 Spin tips

627 were conditioned with 20 µL of solution A (80% acetonitrile, 0,1% TFA), centrifuged at 3,000
628 x g for 2min and equilibrated with 20µL of solution B (75% acetonitrile, 0,075% TFA, 25%
629 lactic acid) followed by centrifugation at 3,000 x g for 2 min. Peptides were resuspended in
630 10 µL of 2% TFA, mixed with 100 µL of solution B and centrifuged at 1,000 x g for 10min.
631 Sample was applied back to the TiO_2 Spin tips two more times in order to increase the
632 adsorption of the phosphopeptides to the TiO_2. Spin tips were washed with, sequentially, 20
633 µL of solution B and two times with 20 µL of solution A. Phosphopeptides were eluted by the
634 sequential addition of 50 µL of 5% NH_4OH and 50 µL of 5% pyrrolidine. Centrifugation was
635 carried out at 1,000 x g for 5 min.
636 Phosphopeptides were further purified using GC Spin tips (GL-Tip, Titansphere, GL Sciences
637 Inc, Japan). Briefly, the GC Spin tips were conditioned with 20 µL of solution A, centrifuged
638 at 3,000 x g for 2 min and equilibrated with 20 µL of solution C (0,1% TFA in HPLC-grade
639 water) followed by centrifugation at 3,000 x g for 2 min. Eluted phosphopeptides from the
640 TiO_2 Spin tips were added to the GC Spin tips and centrifuged at 1,000 x g for 5 min. GC
641 Spin tips were washed with 20 µL of solution C. Phosphopeptides were eluted with 70 µL of
642 solution A (1,000 x g for 3 min) and vacuum dried.
643 ***nanoLC-MS/MS protein identification and quantification.*** Samples were resuspended in
644 12 µL of 0.1% TFA in HPLC-grade water. For each run, 5 µL was injected in a nanoRSLC-Q
645 Exactive PLUS (RSLC Ultimate 3000, Thermo Scientific, MA, USA). Phosphopeptides were
646 loaded onto a µ-precolumn (Acclaim PepMap 100 C18, cartridge, 300 µm i.d.×5 mm, 5 µm,
647 Thermo Scientific, MA, USA) and were separated on a 50 cm reversed-phase liquid
648 chromatographic column (0.075 mm ID, Acclaim PepMap 100, C18, 2 µm, Thermo Scientific,
649 MA, USA). Chromatography solvents were (A) 0.1% formic acid in water, and (B) 80%
650 acetonitrile, 0.08% formic acid. Phosphopeptides were eluted from the column with the
651 following gradient 5% to 40% B (180 min), 40% to 80% (6 min). At 181 min, the gradient
652 returned to 5% to re-equilibrate the column for 20 minutes before the next injection. Two
653 blanks were run between each sample to prevent sample carryover. Phosphopeptides
654 eluting from the column were analyzed by data dependent MS/MS, using top-8 acquisition

655 method. Phosphopeptides were fragmented using higher-energy collisional dissociation
656 (HCD). Briefly, the instrument settings were as follows: resolution was set to 70,000 for MS
657 scans and 17,500 for the data dependent MS/MS scans in order to increase speed. The MS
658 AGC target was set to 1 x 10^6 counts with maximum injection time set to 250 ms, while
659 MS/MS AGC target was set to 2 x 10^5 with maximum injection time set to 250 ms. The MS
660 scan range was from 400 to 1.800 m/z. MS and MS/MS scans were recorded in profile
661 mode. Dynamic exclusion was set to 30 seconds.

662 ***Data Processing Following nanoLC-MS/MS acquisition.*** The MS files were processed
663 with the MaxQuant software version 1.5.3.30 and searched with Andromeda search engine
664 against the UniProtKB/Swiss-Prot *F. tularensis* subsp. *novicida* database (release 28-04-
665 2014, 1719 entries). To search parent mass and fragment ions, we set an initial mass
666 deviation of 4.5 ppm and 0.5 Da respectively. The minimum peptide length was set to 7
667 amino acids and strict specificity for trypsin cleavage was required, allowing up to two missed
668 cleavage sites. Carbamidomethylation (Cys) was set as fixed modification, whereas oxidation
669 (Met), N-term acetylation and phosphorylation (Ser, Thr, Tyr) were set as variable
670 modifications. The match between runs option was enabled with a match time window of 0.7
671 min and an alignment time window of 20 min. The false discovery rates (FDRs) at the protein
672 and peptide level were set to 1%. Scores were calculated in MaxQuant as described
673 previously(Cox & Mann, 2008). The reverse and common contaminants hits were removed
674 from MaxQuant output.

675 The phosphopeptides output table and the corresponding logarithmic intensities were used
676 for phosphopeptide analysis. The phosphopeptide table was expanded to separate individual
677 phosphosites, and we kept all sites identified at least once in the three independent
678 replicates of the analysis of *F. novicida*.

679 All data analysis of mass spectrometry data was performed in Perseus 1.6.0.7. For functional
680 class annotation, we also integrated COG and EggNog databases in Perseus 1.6.0.7, freely

681 available at www.perseus-framework.org. Data are available via ProteomeXchange with
682 identifier PXD009225.

683

684 **Cell cultures and cell infection experiments**

685 J774A.1 (ATCC® TIB-67™) cells were propagated in Dulbecco's Modified Eagle's Medium
686 (DMEM, PAA), containing 10% fetal bovine serum (FBS, PAA) unless otherwise stated. The
687 day before infection, approximately $2x10^5$ eukaryotic cells per well were seeded in 12-well
688 cell tissue plates and bacterial strains were grown overnight in 5 mL of Schaedler K3 at
689 37°C. Infections were realized at a multiplicity of infection (MOI) of 100 and incubated for 1 h
690 at 37°C in culture medium. After 3 washes with cellular culture medium, plates were
691 incubated for 4, 10 and 24 h in fresh medium supplemented with gentamycin (10 µg mL^{-1}). At
692 each kinetic point, cells were washed 3 times with culture medium and lysed by addition of 1
693 mL of distilled water for 10 min at 4°C. The titre of viable bacteria was determined by
694 spreading preparations on chocolate plates. Each experiment was conducted at least twice
695 in triplicates.

696

697 **Time lapse microscopy**

698 J774-1 cells were transduced with the IncuCyte® NucLight Red Lentivirus, following the
699 manufacturer's recommendations, to obtain red nuclear labelling of living cells due to the
700 expression of the red fluorescent protein mKate2 containing a nuclear localization signal.
701 One prior to infection, J774-1 cells were seeded in 12-well cell tissue plates. Cells were
702 infected (MOI of 1,000) with wild-type and mutant GFP-expressing cell. Synchronization of
703 bacterial entry was realized by a 5 minutes centrifugation at 1,000 rpm. Plates were then
704 incubated for 1 h at 37°C in culture medium. After 3 washes with cellular culture medium,
705 plates were incubated at 5% CO_2 and 37°C for 24 hours in fresh medium supplemented with
706 gentamycin (10 µg mL^{-1}). Bacterial multiplication was monitored in the fully automated
707 microscope Incucyte® S3 (Essen BioScience). Images were taken every 20 minutes with the

708 20X objective. Analysis and time-lapse videos (from which images were extracted) were
709 generated by using Incucyte® S3 software.
710

711 **Confocal experiments**

712 J774.1 macrophage cells were infected (MOI of 1,000) with wild-type *F. novicida* U112, the
713 isogenic Δ*iglB* mutant, the Δ*iglB* complemented either with wild-type *iglB* (CpWT) Y139A,
714 Y139F mutants or an isogenic Δ*FPI* strain, in standard DMEM (DMEM-glucose) for 30 min at
715 37°C. Cells were then washed three times with PBS and maintained in fresh DMEM
716 supplemented with gentamycin (10 μg mL^{-1}) until the end of the experiment. Three kinetic
717 points (*i.e.* 1 h, 4 h and 10 h) were sampled. For each time point, cells were washed with 1X
718 PBS, fixed 15 min with 4% paraformaldheyde, and incubated 10 min in 50 mM NH_4Cl in 1X
719 PBS to quench free aldehydes. Cells were then blocked and permeabilised with PBS
720 containing 0.1% saponin and 5% goat serum for 10 min at room temperature. Cells were
721 then incubated for 30 min with anti-*F. novicida* mouse monoclonal antibody (1/500e final
722 dilution, Creative Diagnostics) and anti-LAMP1 rabbit polyclonal antibody (1/100e, ABCAM).
723 After washing, cells were incubated for 30 min with Alexa488-conjugated goat anti mouse
724 and Alexa546 conjugated donkey anti rabbit secondary antibodies (1/400e, AbCam). After
725 washing, DAPI was added (1/1,000) for 1 min and glass coverslips were mounted in Mowiol
726 (Cityfluor Ltd.). Cells were examined using an X63 oil-immersion objective on a Zeiss
727 Apotome 2 microscope. Co-localisation tests were quantified by using Image J software; and
728 mean numbers were calculated on more than 500 cells for each condition. Confocal
729 microscopy analyses were performed at the Cell Imaging Facility (Faculté de Médecine
730 Necker Enfants-Malades).
731

732 **BMDMs Infections**

733 Infection of WT or *ASC*$^{-/-}$ BMDMs was performed as described previously (Rigard et al.,
734 2016). Briefly, BMDMs were differentiated in DMEM (Invitrogen) with 10% v/v FCS (Thermo

735 Fisher Scientific), 15% MCSF (L929 cell supernatant), 10 mM HEPES (Invitrogen), and non-
736 essential amino acids (Invitrogen). One day before infection, macrophages were seeded into
737 12- 48- or 96-well plates at a density of 2 x10^5, 1.5 x10^5 or 5 x10^4 cells per well, respectively
738 and incubated at 37°C, 5% CO_2. The overnight culture of bacteria was added to the
739 macrophages at multiplicity of infection (MOI) of 100. The plates were centrifuged for 15 min
740 at 500 g to ensure comparable adhesion of the bacteria to the cells and placed at 37°C for
741 1h. After 3 washes with PBS, fresh medium with 5 µg mL^{-1} gentamycin (Invitrogen) was
742 added to kill extracellular bacteria and plates were incubated for the desired time.
743

744 **Phagosomal rupture assay**

745 Quantification of vacuolar escape using the β-lactamase/CCF4 assay (Life technologies) was
746 performed as previously described(Meunier, Wallet et al.). *ASC*$^{-/-}$ BMDMs seeded onto non-
747 treated plates were infected as described above for 2 h, washed and incubated in CCF4 for 1
748 h at room temperature in the presence of 2.5 mM probenicid (Sigma). Propidium iodide
749 negative cells were considered for the quantification of cells containing cytosolic *F. novicida*
750 using excitation at 405 nm and detection at 450 nm (cleaved CCF4) or 510 nm (intact CCF4).
751

752 **Mouse infection**

753 We evaluated the impact of the mutations Y139A and Y139F on bacterial virulence in the
754 mouse model of tularemia, using an *in vivo* competition assay (Gesbert et al., 2014). Wild-
755 type *F. novicida*, the Δ*iglB* mutant and the Δ*iglB* mutant complemented either with wild-type
756 *iglB* (CpWT) or with Y139A and Y139F mutants, were grown in Schaedler K3 to exponential
757 growth phase and diluted to the appropriate concentrations. 6 to 8-week-old female BALB/c
758 mice (Janvier, Le Genest St Isle, France) were intraperitoneally (i.p.) inoculated with 200 µL
759 of bacterial suspension. The actual number of viable bacteria in the inoculum was
760 determined by plating dilutions of the bacterial suspension on chocolate plates. For
761 competitive infections, wild-type *F. novicida* and mutant bacteria were mixed in 1:1 ratio and
762 a total of 100 bacteria were used for infection of each of five mice. After two days, mice were

763 sacrificed. Homogenized spleen and liver tissue from the five mice in one experiment were
764 mixed, diluted and spread on to chocolate agar plates. Kanamycin selection to distinguish
765 wild-type and mutant bacteria was performed. The competitive index (CI) was determined as
766 the ratio (mutant output/WT output) / (mutant input/WT input). Statistical analysis for CI
767 experiments was as described in (Brotcke, Weiss et al., 2006). Macrophage experiments
768 were analyzed by using the Student's unpaired t test.
769

770 **Sequence analyses**

771 To retrieve IglB homologous proteins, we used the Hidden Markov Model (HMM) profile
772 "T6SSii_iglB.hmm" from reference (Abby et al., 2016). We scanned a dataset of 2,462
773 predicted proteomes of complete bacterial genomes retrieved from GenBank Refseq (last
774 accessed September 2016) using *hmmsearch* program of HMMER v.3.1b2 (gathering
775 threshold = 25).
776 Our dataset included 19 genomes of the *Francisella* genus. All IglB sequences encoded by
777 *Francisella* genomes were aligned with MUSCLE v.3.8.31 (Edgar, 2004). Due to differences
778 in the annotation of the first methionine codon, we used the sequence of FTN_1323 as a
779 reference for the multiple sequence alignment.
780 Redundancy of the sequence set retrieved from *hmmsearch* was reduced using cd-hit-
781 v4.6.7 (Fu, Niu et al., 2012) with a 90% identity threshold. The longest representative
782 sequence of each cluster was then aligned with MUSCLE v.3.8.31 (Edgar, 2004). Outliers
783 that were very divergent in sequence length were removed. PROMALS3D and ESPript3.0
784 (Robert & Gouet, 2014) servers were used to visualize multiple sequence and structure
785 alignment using 3J9O.B PDB structure reference file (Clemens et al., 2015). To determine
786 the conservation of the phosphotyrosine site identified in *Francisella* genus (Tyr139 or Y139)
787 we focused on the 12 amino acids surrounding the *Francisella* Tyr139 residue in the 535
788 aligned sequences.
789 To determine the conservation of the phosphotyrosine site identified in *Francisella* genus
790 (Tyr139) we focused on the 12 amino acids surrounding the *Francisella* Y139 residue in the

535 aligned sequences. Out of the 535 aligned sequences, we found 90 sequences with a tyrosine residue in the vicinity of *Francisella* Tyr139 residue. For illustrative purpose, we selected 12 representative sequences out of 90 as shown in **Fig. S3**.

Data Availability

The mass spectrometry proteomics data have been deposited to the ProteomeXchange Consortium via the PRIDE (Perez-Riverol, Xu et al., 2016) partner repository with the dataset identifier PXD012507.

Acknowledgements

We thank Dr A. Sjostedt for providing the *Francisella* strain U112 and its *ptpA* transposon insertion derivative (*FTN_1046*) and Alain Schmitt (Cochin Institute Electron Microscopy Facility) for excellent technical support.

Funding

These studies were supported by INSERM, CNRS and Université Paris Descartes Paris Cité Sorbonne. Jason Ziveri was funded by a fellowship from the “Délégation Générale à l’Armement”. Claire Lays was funded by a fellowship from the LABEX ECOFECT (ANR-11-LABX-0048) of Université de Lyon, within the program "Investissement d'Avenir" (ANR-11-IDEX-0007) operated by the French National Research Agency (ANR).

Authors contribution

J.Z. performed most of the in vitro experiments; F.T. performed murine in vivo experiments and some immunofluorescence experiments; I.C.G and C.C. performed the proteomic analyses and I.C.G analyzed and compiled the data; N. K. performed the 3D analysis; A.J. performed the sequence alignments and analyzed the data ; H.R and M.C. performed the time lapse microscopy analyses; G.P. performed some in vitro experiments; M.B. and T.H. analyzed the data ; A.C. designed the experiments and J.Z. and A.C. analyzed the data, and wrote the paper.

The funders had no role in study design, data collection and analysis, decision to publish, or preparation of the manuscript.

Conflict of interest

The authors declare that they have no conflict of interest.

References

Abby SS, Cury J, Guglielmini J, Neron B, Touchon M, Rocha EP (2016) Identification of protein secretion systems in bacterial genomes. Sci Rep 6: 23080

Abd H, Johansson T, Golovliov I, Sandstrom G, Forsman M (2003) Survival and growth of Francisella tularensis in Acanthamoeba castellanii. Appl Environ Microbiol 69: 600-6

Aussel L, Pierrel F, Loiseau L, Lombard M, Fontecave M, Barras F (2014) Biosynthesis and physiology of coenzyme Q in bacteria. Biochim Biophys Acta 1837: 1004-11

Baroni S, Pandini V, Vanoni MA, Aliverti A (2012) A single tyrosine hydroxyl group almost entirely controls the NADPH specificity of Plasmodium falciparum ferredoxin-NADP+ reductase. Biochemistry 51: 3819-26

844 Bolen DW, Rose GD (2008) Structure and energetics of the hydrogen-bonded backbone in
845 protein folding. Annu Rev Biochem 77: 339-62
846 Brodmann M, Dreier RF, Broz P, Basler M (2017) Francisella requires dynamic type VI
847 secretion system and ClpB to deliver effectors for phagosomal escape. Nat Commun 8:
848 15853
849 Broms JE, Lavander M, Sjostedt A (2009) A conserved alpha-helix essential for a type VI
850 secretion-like system of Francisella tularensis. J Bacteriol 191: 2431-46
851 Broms JE, Sjostedt A, Lavander M (2010) The Role of the Francisella Tularensis
852 Pathogenicity Island in Type VI Secretion, Intracellular Survival, and Modulation of Host Cell
853 Signaling. Front Microbiol 1: 136
854 Brotcke A, Weiss DS, Kim CC, Chain P, Malfatti S, Garcia E, Monack DM (2006)
855 Identification of MglA-regulated genes reveals novel virulence factors in Francisella
856 tularensis. Infect Immun 74: 6642-55
857 Celli J, Zahrt TC (2013) Mechanisms of Francisella tularensis intracellular pathogenesis.
858 Cold Spring Harb Perspect Med 3: a010314
859 Chamberlain RE (1965) Evaluation of Live Tularemia Vaccine Prepared in a Chemically
860 Defined Medium. Appl Microbiol 13: 232-5
861 Charity JC, Blalock LT, Costante-Hamm MM, Kasper DL, Dove SL (2009) Small molecule
862 control of virulence gene expression in Francisella tularensis. PLoS Pathog 5: e1000641
863 Cianfanelli FR, Monlezun L, Coulthurst SJ (2016) Aim, Load, Fire: The Type VI Secretion
864 System, a Bacterial Nanoweapon. Trends Microbiol 24: 51-62
865 Clemens DL, Ge P, Lee BY, Horwitz MA, Zhou ZH (2015) Atomic structure of T6SS reveals
866 interlaced array essential to function. Cell 160: 940-951
867 Clemens DL, Lee BY, Horwitz MA (2018) The Francisella Type VI Secretion System. Front
868 Cell Infect Microbiol 8: 121
869 Cox J, Mann M (2008) MaxQuant enables high peptide identification rates, individualized
870 p.p.b.-range mass accuracies and proteome-wide protein quantification. Nat Biotechnol 26:
871 1367-72

872 Cuthbert BJ, Ross W, Rohlfing AE, Dove SL, Gourse RL, Brennan RG, Schumacher MA
873 (2017) Dissection of the molecular circuitry controlling virulence in Francisella tularensis.
874 Genes Dev 31: 1549-1560
875 Dudkiewicz M, Szczepinska T, Grynberg M, Pawlowski K (2012) A novel protein kinase-like
876 domain in a selenoprotein, widespread in the tree of life. PLoS One 7: e32138
877 Edgar RC (2004) MUSCLE: a multiple sequence alignment method with reduced time and
878 space complexity. BMC Bioinformatics 5: 113
879 Eshraghi A, Kim J, Walls AC, Ledvina HE, Miller CN, Ramsey KM, Whitney JC, Radey MC,
880 Peterson SB, Ruhland BR, Tran BQ, Goo YA, Goodlett DR, Dove SL, Celli J, Veesler D,
881 Mougous JD (2016) Secreted Effectors Encoded within and outside of the Francisella
882 Pathogenicity Island Promote Intramacrophage Growth. Cell Host Microbe 20: 573-583
883 Fu L, Niu B, Zhu Z, Wu S, Li W (2012) CD-HIT: accelerated for clustering the next-generation
884 sequencing data. Bioinformatics 28: 3150-2
885 Gallagher LA, Ramage E, Jacobs MA, Kaul R, Brittnacher M, Manoil C (2007) A
886 comprehensive transposon mutant library of Francisella novicida, a bioweapon surrogate.
887 Proc Natl Acad Sci U S A 104: 1009-14
888 Gesbert G, Ramond E, Rigard M, Frapy E, Dupuis M, Dubail I, Barel M, Henry T, Meibom K,
889 Charbit A (2014) Asparagine assimilation is critical for intracellular replication and
890 dissemination of Francisella. Cell Microbiol 16: 434-49
891 Gesbert G, Ramond E, Tros F, Dairou J, Frapy E, Barel M, Charbit A (2015) Importance of
892 branched-chain amino acid utilization in Francisella intracellular adaptation. Infect Immun 83:
893 173-83
894 Kingry LC, Petersen JM (2014) Comparative review of Francisella tularensis and Francisella
895 novicida. Front Cell Infect Microbiol 4: 35
896 Kiss K, Liu W, Huntley JF, Norgard MV, Hansen EJ (2008) Characterization of fig operon
897 mutants of Francisella novicida U112. FEMS Microbiol Lett 285: 270-7
898 Klionsky DJ, Abdelmohsen K, Abe A, Abedin MJ, Abeliovich H, Acevedo Arozena A, Adachi
899 H, Adams CM, Adams PD, Adeli K, Adhihetty PJ, Adler SG, Agam G, Agarwal R, Aghi MK,

900 Agnello M, Agostinis P, Aguilar PV, Aguirre-Ghiso J, Airoldi EM et al. (2016) Guidelines for
901 the use and interpretation of assays for monitoring autophagy (3rd edition). Autophagy 12: 1-
902 222
903 Lagrange B, Benaoudia S, Wallet P, Magnotti F, Provost A, Michal F, Martin A, Di Lorenzo F,
904 Py BF, Molinaro A, Henry T (2018) Human caspase-4 detects tetra-acylated LPS and
905 cytosolic Francisella and functions differently from murine caspase-11. Nat Commun 9: 242
906 Lauriano CM, Barker JR, Yoon SS, Nano FE, Arulanandam BP, Hassett DJ, Klose KE (2004)
907 MglA regulates transcription of virulence factors necessary for Francisella tularensis
908 intraamoebae and intramacrophage survival. Proc Natl Acad Sci U S A 101: 4246-9
909 Ledvina HE, Kelly KA, Eshraghi A, Plemel RL, Peterson SB, Lee B, Steele S, Adler M,
910 Kawula TH, Merz AJ, Skerrett SJ, Celli J, Mougous JD (2018) A Phosphatidylinositol 3-
911 Kinase Effector Alters Phagosomal Maturation to Promote Intracellular Growth of Francisella.
912 Cell Host Microbe 24: 285-295 e8
913 Lipecka J, Chhuon C, Bourderioux M, Bessard MA, van Endert P, Edelman A, Guerrera IC
914 (2016) Sensitivity of mass spectrometry analysis depends on the shape of the filtration unit
915 used for filter aided sample preparation (FASP). Proteomics 16: 1852-7
916 Ludu JS, de Bruin OM, Duplantis BN, Schmerk CL, Chou AY, Elkins KL, Nano FE (2008)
917 The Francisella pathogenicity island protein PdpD is required for full virulence and associates
918 with homologues of the type VI secretion system. J Bacteriol 190: 4584-95
919 Luque-Larena JJ, Mougeot F, Arroyo B, Vidal MD, Rodriguez-Pastor R, Escudero R, Anda P,
920 Lambin X (2017) Irruptive mammal host populations shape tularemia epidemiology. PLoS
921 Pathog 13: e1006622
922 Maurin M, Gyuranecz M (2016) Tularaemia: clinical aspects in Europe. Lancet Infect Dis 16:
923 113-124
924 McLendon MK, Apicella MA, Allen LA (2006) Francisella tularensis: taxonomy, genetics, and
925 Immunopathogenesis of a potential agent of biowarfare. Annu Rev Microbiol 60: 167-85
926 Meibom KL, Barel M, Charbit A (2009) Loops and networks in control of Francisella
927 tularensis virulence. Future Microbiol 4: 713-29

928 Mettert EL, Kiley PJ (2015) How Is Fe-S Cluster Formation Regulated? Annu Rev Microbiol
929 69: 505-26
930 Meunier E, Wallet P, Dreier RF, Costanzo S, Anton L, Ruhl S, Dussurgey S, Dick MS,
931 Kistner A, Rigard M, Degrandi D, Pfeffer K, Yamamoto M, Henry T, Broz P (2015)
932 Guanylate-binding proteins promote activation of the AIM2 inflammasome during infection
933 with Francisella novicida. Nat Immunol 16: 476-484
934 Meyer L, Broms JE, Liu X, Rottenberg ME, Sjostedt A (2015) Microinjection of Francisella
935 tularensis and Listeria monocytogenes reveals the importance of bacterial and host factors
936 for successful replication. Infect Immun 83: 3233-42
937 Mougous JD, Gifford CA, Ramsdell TL, Mekalanos JJ (2007) Threonine phosphorylation
938 post-translationally regulates protein secretion in Pseudomonas aeruginosa. Nat Cell Biol 9:
939 797-803
940 Nano FE, Zhang N, Cowley SC, Klose KE, Cheung KK, Roberts MJ, Ludu JS, Letendre GW,
941 Meierovics AI, Stephens G, Elkins KL (2004) A Francisella tularensis pathogenicity island
942 required for intramacrophage growth. J Bacteriol 186: 6430-6
943 Nazarov S, Schneider JP, Brackmann M, Goldie KN, Stahlberg H, Basler M (2018) Cryo-EM
944 reconstruction of Type VI secretion system baseplate and sheath distal end. EMBO J 37
945 Nguyen VS, Douzi B, Durand E, Roussel A, Cascales E, Cambillau C (2018) Towards a
946 complete structural deciphering of Type VI secretion system. Curr Opin Struct Biol 49: 77-84
947 Ostrowski A, Cianfanelli FR, Porter M, Mariano G, Peltier J, Wong JJ, Swedlow JR, Trost M,
948 Coulthurst SJ (2018) Killing with proficiency: Integrated post-translational regulation of an
949 offensive Type VI secretion system. PLoS Pathog 14: e1007230
950 Pace CN, Horn G, Hebert EJ, Bechert J, Shaw K, Urbanikova L, Scholtz JM, Sevcik J (2001)
951 Tyrosine hydrogen bonds make a large contribution to protein stability. J Mol Biol 312: 393-
952 404
953 Perez-Riverol Y, Xu QW, Wang R, Uszkoreit J, Griss J, Sanchez A, Reisinger F, Csordas A,
954 Ternent T, Del-Toro N, Dianes JA, Eisenacher M, Hermjakob H, Vizcaino JA (2016) PRIDE
955 Inspector Toolsuite: Moving Toward a Universal Visualization Tool for Proteomics Data

956 Standard Formats and Quality Assessment of ProteomeXchange Datasets. Mol Cell
957 Proteomics 15: 305-17
958 Pizarro-Cerda J, Charbit A, Enninga J, Lafont F, Cossart P (2016) Manipulation of host
959 membranes by the bacterial pathogens Listeria, Francisella, Shigella and Yersinia. Semin
960 Cell Dev Biol
961 Ramond E, Gesbert G, Guerrera IC, Chhuon C, Dupuis M, Rigard M, Henry T, Barel M,
962 Charbit A (2015) Importance of host cell arginine uptake in Francisella phagosomal escape
963 and ribosomal protein amounts. Mol Cell Proteomics 14: 870-81
964 Ramsey KM, Osborne ML, Vvedenskaya IO, Su C, Nickels BE, Dove SL (2015) Ubiquitous
965 promoter-localization of essential virulence regulators in Francisella tularensis. PLoS Pathog
966 11: e1004793
967 Rigard M, Broms JE, Mosnier A, Hologne M, Martin A, Lindgren L, Punginelli C, Lays C,
968 Walker O, Charbit A, Telouk P, Conlan W, Terradot L, Sjostedt A, Henry T (2016) Francisella
969 tularensis IglG Belongs to a Novel Family of PAAR-Like T6SS Proteins and Harbors a
970 Unique N-terminal Extension Required for Virulence. PLoS Pathog 12: e1005821
971 Robert X, Gouet P (2014) Deciphering key features in protein structures with the new
972 ENDscript server. Nucleic Acids Res 42: W320-4
973 Roche B, Aussel L, Ezraty B, Mandin P, Py B, Barras F (2013) Iron/sulfur proteins biogenesis
974 in prokaryotes: formation, regulation and diversity. Biochim Biophys Acta 1827: 455-69
975 Russell AB, Wexler AG, Harding BN, Whitney JC, Bohn AJ, Goo YA, Tran BQ, Barry NA,
976 Zheng H, Peterson SB, Chou S, Gonen T, Goodlett DR, Goodman AL, Mougous JD (2014) A
977 type VI secretion-related pathway in Bacteroidetes mediates interbacterial antagonism. Cell
978 Host Microbe 16: 227-236
979 Santic M, Molmeret M, Klose KE, Abu Kwaik Y (2006) Francisella tularensis travels a novel,
980 twisted road within macrophages. Trends Microbiol 14: 37-44
981 Sjostedt A (2007) Tularemia: history, epidemiology, pathogen physiology, and clinical
982 manifestations. Ann N Y Acad Sci 1105: 1-29

983 Sjostedt A (2011) Francisella tularensis and tularemia. In Fontiers Research Topic Ebooks,
984 Fontiers Media SA
985 Spidlova P, Stulik J (2017) Francisella tularensis type VI secretion system comes of age.
986 Virulence 8: 628-631
987 Stefely JA, Pagliarini DJ (2017) Biochemistry of Mitochondrial Coenzyme Q Biosynthesis.
988 Trends Biochem Sci 42: 824-843
989 Sullivan JT, Jeffery EF, Shannon JD, Ramakrishnan G (2006) Characterization of the
990 siderophore of Francisella tularensis and role of fslA in siderophore production. J Bacteriol
991 188: 3785-95
992 Vettiger A, Basler M (2016) Type VI Secretion System Substrates Are Transferred and
993 Reused among Sister Cells. Cell 167: 99-110 e12
994 Wehrly TD, Chong A, Virtaneva K, Sturdevant DE, Child R, Edwards JA, Brouwer D, Nair V,
995 Fischer ER, Wicke L, Curda AJ, Kupko JJ, 3rd, Martens C, Crane DD, Bosio CM, Porcella
996 SF, Celli J (2009) Intracellular biology and virulence determinants of Francisella tularensis
997 revealed by transcriptional profiling inside macrophages. Cell Microbiol 11: 1128-50
998 Weiss DS, Brotcke A, Henry T, Margolis JJ, Chan K, Monack DM (2007) In vivo negative
999 selection screen identifies genes required for Francisella virulence. Proc Natl Acad Sci U S A
1000 104: 6037-6042
1001 Ziveri J, Barel M, Charbit A (2017) Importance of Metabolic Adaptations in Francisella
1002 Pathogenesis. Front Cell Infect Microbiol 7: 96
1003 Ziveri J, Tros F, Guerrera IC, Chhuon C, Audry M, Dupuis M, Barel M, Korniotis S, Fillatreau
1004 S, Gales L, Cahoreau E, Charbit A (2017) The metabolic enzyme fructose-1,6-bisphosphate
1005 aldolase acts as a transcriptional regulator in pathogenic Francisella. Nat Commun 8: 853
1006
1007
1008

1009 # Figure legends

1010

1011

1012 **Figure 1. KCl stimulation of sheath formation**

1013 (**A**) Sucrose gradient. Lysates of bacteria grown in Schaedler K3 medium in the presence of KCl were
1014 laid on top of a discontinuous sucrose gradient 15%-55%/Optiprep 55%. Left panel, composition of
1015 the gradient; Right panel, transmission electron microscopy (TEM) of the "heavy" fraction (grey arrow,
1016 topping the Optiprep cushion). The assembled sheath-like structure, sedimenting at equilibrium to
1017 below 55% sucrose, showed rod-shaped particles of variable length (100 - 600 nm). (**B**) Western
1018 blotting analysis of the different fractions, using anti-Igl (A, B or C) antibodies. (**C**) The proteome of
1019 KCl-stimulated and non-stimulated *F. novicida.* Volcano plot representing the statistical
1020 comparison of the protein LFQ intensities of KCl- stimulation vs non-stimulated cells. Inner
1021 volcano was established using S0=0.5, FDR=0.01 (class B proteins) and the outer volcano
1022 using S0=0.5, FDR=0.001 (class A proteins). Proteins belonging to the FPI, the Fe uptale
1023 and Fe-S clusters are highlighted in color as indicated.

1024

1025 **Figure 2. The phosphoproteome of *F. novicida***

1026 (A) Distribution of phosphosites according to the modified amino acid (tyrosine,Y; threonine,
1027 T and serine, S). (B) Histograms of the most represented classes of protein. The values
1028 correspond to the number of proteins bearing phosphosites in each category. (C) Heat map
1029 of phosphoproteins altered upon KCl stimulation (Pink to right of the FTN numbers
1030 corresponds to proteins with multiple phosphorylation sites). (D) IglB phosphorylation
1031 distribution. Intensities (in log2) of the non phosphorylated (left) and phosphorylated (right)
1032 Tyr139-containing peptide in the "heavy" (H) and "light" (L) fractions. The signal of the
1033 phosphopeptide was only detectable after phosphoenrichment. nd, not detectable.

1034

1035 **Figure 3. Predicted role of Y139 of IglB in sheath assembly**

1036 (**A**) Overview of the sheath that consists of 12 helical strands based on EM reconstruction at
1037 3.7 Å. Each unit consists of a IglA/IglB dimer. The same colors were used in the further
1038 pictures. The chains near Tyr139 of IglB consist of 2 IglA/IglB dimers from the same strand
1039 (pink/grey and coral/sky blue). The N-terminal tail of an IglA (blue) from an adjacent strand
1040 wraps round to close to Y139 of this strand. (**B**) A closer view of just the selected chains.
1041 (**C**) Close up of the region of Tyr139. The hydroxyl is pointing into a pocket and not
1042 obviously making a Hydrogen bond. However, the carboxylates of Asp114 from IglB and
1043 Asp63 of IglA in the next dimer are around 5 Å away. At the resolution of the reconstruction
1044 side chain density is not well defined and these could in fact be close enough to H bond.
1045 (**D**) Surface of the assembly clipped to show Tyr139. There is enough space for a Phospho
1046 group on the Tyr. The two Asps will however be close to the phosphogroup and so there is
1047 likely to be charge repulsion impairing the sheath assembly or weakening the sheath stability
1048 when Y139 is phosphorylated.

1049

1050 **Figure 4. Immunodetection of IglA, IglB and IglC in wild-type and IglB mutant**
1051 **strains**

1052 (**A**) Western Blots (WB) of whole cell protein extracts. Upper gel: WB with anti-IglB; lower
1053 gel: WB with anti-IglA. (**B**) Western Blots (WB) with anti-IglC on bacteria / culture filtrates.
1054 Bacteria were grown in Schaedler-K3 supplemented or not with 5% KCl until late log phase
1055 and then harvested by centrifugation. Culture supernatants were collected after filtration on
1056 0.2 µM Millipore filters and concentrated using Amicon 3 kDa membranes. The equivalent of
1057 200 µg of total protein were loaded onto each well. Upper gel, bacterial cultures grown
1058 without KCl; lower gel, bacterial cultures supplemented with 5% KCl. (**C**) Co-
1059 immunoprecipitations (Co-IP). Upper gel: IP-anti-IglA, followed by WB with anti-IglB; lower
1060 gel: IP-anti-IglB, followed by WB with anti-IglA. (**D**) WBs of sucrose gradient fractions of the
1061 Y139F and Y139A mutant strains. **(E)** Distribution of the intensities (trasformed in log 2) of

1062 the proteins IglA and IglB in the Heavy (H) and light (L) sucrose fraction, in cp WT (Δ*iglB*
1063 complemented with WT IglB), Y139F and Y139A (Δ*iglB* complemented with IglB Y139F and
1064 IglB Y139A, respectively).

1065

1066 **Figure 5. Y139Aand Y139F IglB mutants show impaired intracellular survival**
1067 **and attenuated virulence**

1068 (**A**) Intracellular bacterial multiplication of wild-type *F. novicida* (WT, Grey squares), isogenic
1069 Δ*iglB* mutant (Δ*iglB*, blue triangles) and complemented Δ*iglB* strain (Cp-WT, grey circles;
1070 Y139A, blue square; Y139F, red squares) and the Δ*FPI* control (black lines), was monitored
1071 during 24 h in J774A.1 macrophage cells. The values recorded for Y139F, at 24 h, were
1072 significantly different from those of Δ*FPI*, Δ*iglB* or Y139A. In both cell types, the values
1073 recorded for WT or CpWT, at 10 h and 24 h, were significantly different from those of Δ*FPI*,
1074 Δ*iglB,* Y139A or Y139F. **p<0.001 (determined by student's t-test). (**B**) Confocal microscopy
1075 of intracellular bacteria with J774-1 infected with wild-type *F. novicida* (WT), Δ*iglB* or
1076 complemented strains and their co-localization with the phagosomal marker LAMP1
1077 observed at 1 h, 4 h and 10 h. Upper par: J774.1 were stained for *F. novicida* (green), LAMP-
1078 1 (red) and host DNA (blue, DAPI stained). Lower part: analysis was performed with ImageJ
1079 software. *p<0.01 (determined by student's t-test).

1080

1081

1082 **Figure 6. Electron microscopy and time lapse video microscopy**

1083 (**A**) Transmission electron microscopy of J774-1 cells infected with Y139F, Y139A or WT *F.*
1084 *novicida* at 24 h. Black arrowheads (in cells infected with Y139A) point to single bacteria. (**B**)
1085 Time lapse video microscopy. J774-1 cells expressing a nuclear restricted Red Fluorescent
1086 Protein were infected with GFP-expressing WT and Y139 IglB proteins. Representative

1087 images were taken at 4,h, 8 h and 20 h (see Video S1 and S2). Red: cell nuclei. Green: GFP
1088 expressing bacteria.

1089

1090 **Figure 7. Proposed model of phosphorylation-dependent TSS6 disassembly**

1091 Upon bacterial entry into the phagosomal compartment, non-phosphorylated IglB form stable
1092 heterodimers with IglA and sheath polymerization initiates at the bacterial pole. Within 30 min,
1093 T6SS sheath contraction triggers the secretion of effectors and the rupture of the
1094 phagosomal membrane. Immediately after, the T6SS sheath disassembles, thanks to the
1095 concerted action of the ClpB unfoldase and of the phosphorylation of IglB residue Y139.

1096

1097

1098 # Supplementary materials

1099

1100 **Figure supplement 1. Schematic representation of the FPI locus and overview**
1101 **of the T6SS structure of *Francisella***

1102 The *Francisella* FPI locus representation (*anmK* to *pdpA* gene) with nomenclature of the
1103 canonical T6SS and the *F. novicida* T6SS. A color was assigned for each gene function and
1104 applied on the overview of the T6SS structure. Red/Green/Blue/Orange, structural protein;
1105 Grey, secreted protein; White, hypothetical protein

1106

1107 **Figure supplement 2. Schematic representation of the genomic regions**
1108 **encoding proteins whose expression vary upon KCl stimulation.**

1109 (**A**) Genomic organization of the FNI; (**B**). the Fe-S cluster- and iron uptake-associated loci.
1110 Genes colored in blue correspond to proteins present in decreased amounts; genes colored
1111 in rose, to proteins present in increased amounts, genes in white, unchanged.

1112

1113 **Figure supplement 3. Alignments of orthologous IglB proteins**

1114 (**A**) Alignments of orthologous IglBs proteins showing conservation of Y139 in *Francisellae*.
1115 The IglB sequences retrieved from 19 *Francisella* genomes were aligned using MUSCLE
1116 (Edgar, 2004) and rendered using ESPript3.0 (Robert & Gouet, 2014). Secondary structure
1117 elements information is extracted from 3J9O PDB file (Clemens et al., 2015) and is displayed
1118 at the top of the alignment. Sequences are identified by corresponding species name
1119 followed by strain name and locus tag. Species names are abbreviated as follow: Fn,
1120 *Francisella tularensis* subsp. *novicida*; Ftm, *Francisella tularensis* subsp. *mediasiatica*; Fth,
1121 *Francisella tularensis* subsp. *holarctica*; Ftt, *Francisella tularensis* subsp. *tularensis*; Ft,
1122 *Francisella tularensis*; Fno, *Francisella noatunensis*; Fsp, *Francisella* sp. (**B**) Alignments of
1123 orthologous IglBs in other genera showing conservation of a tyrosine residue. Sequences of

1124 11 representative IglB orthologs with a tyrosine residue in the vicinity of Y139 were aligned
1125 using MUSCLE (Edgar, 2004) and rendered using ESPript3.0 (Robert & Gouet, 2014).
1126 Secondary structure elements information is extracted from 3J9O PDB file (Clemens et al.,
1127 2015) and is displayed at the top of the alignment. Sequences are identified by
1128 corresponding Uniprot accession number. Species names are abbreviated as follow: FRATN,
1129 *Francisella tularensis subsp. novicida*; SALTY, *Salmonella* Typhimurium; YERPE, *Yersinia*
1130 *pestis; BURMA, Burkholderia mallei; XANC5, Xanthomonas campestris; RALP1, Ralstonia*
1131 *pickettii; PHOAA, Photorhabdus asymbiotica; ERWAC, Erwinia amylovora; ENTCC,*
1132 *Enterobacter cloacae; BRAJP, Bradyrhizobium japonicum; RHIFR, Rhizobium fredii;*
1133 *9GAMM, Serratia nematodiphila.*

1134

1135 **Figure supplement 4. Effect of IglB mutations on growth in broth**

1136 Wild-type *F. novicida* (WT, Grey squares), isogenic Δ*iglB* mutant (Δ*iglB*, blue triangles), and
1137 complemented *iglB* strain (Cp-WT, grey circles; Y139A, purple square; Y139F, red
1138 square), were grown in Schaedler K3 (left panel) or in Tryptic Soy broth (TSB) supplemented
1139 with 0,2% cysteine (right panel).

1140

1141 **Figure supplement 5. Intracellular multiplication in bone marrow-derived**
1142 **macrophages**

1143 (**A**) Intracellular bacterial multiplication of wild-type *F. novicida* (WT, Grey squares), isogenic Δ*iglB*
1144 mutant (Δ*iglB*, blue triangles) and complemented Δ*iglB* strain in bone marrow-derived macrophages
1145 (BMDM) from BALB/c mice. (**B**) CCF4 assay. Infection of *ASC*$^{-/-}$BMDM were performed at MOI of 100
1146 and the cytosol of BMDMs was loaded with CCF4, as described previously (Ramond et al., 2015). *F.*
1147 *novicida* naturally expresses a β-lactamase able to cleave the CCF4. Bacterial escape into the host
1148 cytosol is thus associated with a shift of the CCF4 probe fluorescence emission from 535 nm to 450
1149 nm. The number of cells demonstrating CCF4 cleavage, determined at different time points (1 h, 3 h
1150 and 6 h) by flow cytometry, reached above 50% at 6 h for both WT and CpWT complemented strains

1151 whereas it was below 1% for the other mutant strains tested. (**C**) Groups of five female BALB/c
1152 mice were infected intraperitoneally with a mixture of 100 CFU of wild-type *F. novicida* and
1153 100 CFU of Δ*iglB* mutant strain or complemented strain (Cp-WT, Y139A, Y139F). Bacterial
1154 burden was quantified in liver (L) and spleen (S) of mice. The data represent the competitive
1155 index (CI) value (in ordinate) for CFU of mutant/wild-type of each mouse, after 48 h infection,
1156 divided by CFU of mutant/wild-type in the inoculum. The CI recorded for the two *iglB* mutants
1157 was very low in both spleen and livers 2.5 days after infection (close to 10^{-7}). As a control, we
1158 also performed an *in vivo* competition assay between wild-type and the Δ*iglB* complemented
1159 strain (WT and CpWT). The competition index recorded close to 1 for CpWT (≤10^{-1} in both
1160 target organs), confirmed almost complete functional complementation.
1161 Bars represent the geometric mean CI value.
1162

1163 **Figure supplement 6. Substitution of Tyr139 by phosphomimetics (Glu or Asp)**

1164 (**A**) J774.1 macrophage-like cells were infected in DMEM with 100 MOI of wild-type *F.*
1165 *novicida* (WT) and mutated strains (Y139E, Y139D, Δ*FPI*) for 24 h. Results are shown as the
1166 average of $\log_{10}$ cfu mL^{-1} ± standard deviation. Each experiment was performed in triplicate.
1167 **, p<0.001 (as determined by two-tailed unpaired Student's *t*-test). (**B**) WB with anti-IglB of
1168 sucrose gradient fractions.

1169 **Figure supplement 7. Inactivation of genes encoding proteins bearing a**
1170 **putative tyrosine kinase domain**

1171 J774.1 macrophage-like cells were infected in DMEM-High glucose with an MOI of 100 with
1172 wild-type *F. novicida* (WT), three mutants corresponding to a transposon insertion into genes
1173 *FTN_1082*, *FTN_1433*, *FTN_0459* (tnfn1_pw060323p01q162, tnfn1_pw060420p02q142,
1174 tnfn1_pw060323p07q132, respectively from the BEI resources repository), here designated
1175 Δ*1082*, Δ*1433*, Δ*0459,* for simplification), and a Δ*FPI* mutant (Δ*FPI*). Intracellular

1176 multiplication was monitored at 10 h. Results are shown as the average of log10 cfu mL^{-1} ±
1177 standard deviation. Each experiment was performed in triplicate.
1178

1179

1180 **Video supplement 1.** WT: J774.1 macrophage-like cells were infected in DMEM-High
1181 glucose at an MOI of 1,000 with wild-type *F. novicida* Δ*iglB* expressing pKK214::pGro*iglB*-
1182 pGro*gfp* (designated cpWT-GFP).
1183

1184 **Video supplement 2.** Y139F: J774.1 macrophage-like cells were infected in DMEM-High
1185 glucose at an MOI of 1,000 with wild-type *F. novicida* Δ*iglB* expressing
1186 pKK214::pGro*iglB*Y139F-pGro*gfp* (designated cpY139F-GFP)
1187

1188

1189 **Table supplement 1. Whole cell proteome of non-induced and KCl-induced *F.***
1190 ***novicida.*** In this table, we report the log2 (intensity) of the proteins identified in whole cell
1191 fractions from non-induced and KCl-induced wild-type *F. novicida*. Peptides and sequence
1192 coverage indicates the number of total peptides identified and the primary sequence
1193 coverage for that protein across samples. The Q value and the score refer to the quality of
1194 the identification.

1195 **Table supplement 2. Detailed list of phosphosites identified in *F. novicida***
1196 In this table, we report: i) the average of the log2 (intensity) of the phosphosites identified
1197 from three independent replicates; ii) the amino acid carrying the phosphorylation ("Amino
1198 Acid"); iii) its position on the protein (Position); iv) the "localization probability" of the
1199 phosphosite (1 being 100%); v) the number of replicates the phosphosite has been identified
1200 in ("identified"); vi) the "sequence window" of 15 amino acids before and after the amino acid
1201 phosphorylated; vii) the probability and score of identification and localization (PEP, score,

1202 score for localization); viii) the "charge" of the peptide; and ix) the annotation according to
1203 COG and EggNOG.
1204
1205 **Table supplement 3. Table of intensities for IglB peptide carrying Y139**
1206 **phosphorylation.**
1207
1208 **Table supplement 4. List of proteins identified in the "Heavy" (H) and "Light"**
1209 **(L) Fraction in WT and in the Y139F mutant**
1210 WT_H, WT_L, Y139_H, Y139F_L report the log2 (intensity) of the proteins identified in the
1211 fractions. Peptides and sequence coverage indicates the number of total peptides identified
1212 and the primary sequence coverage for that protein across samples. The Q value and the
1213 score refer to the quality of the identification.
1214
1215 **Table supplement 5. Strains and plasmids.**
1216
1217 **Table supplement 6. Primers.**
1218
1219

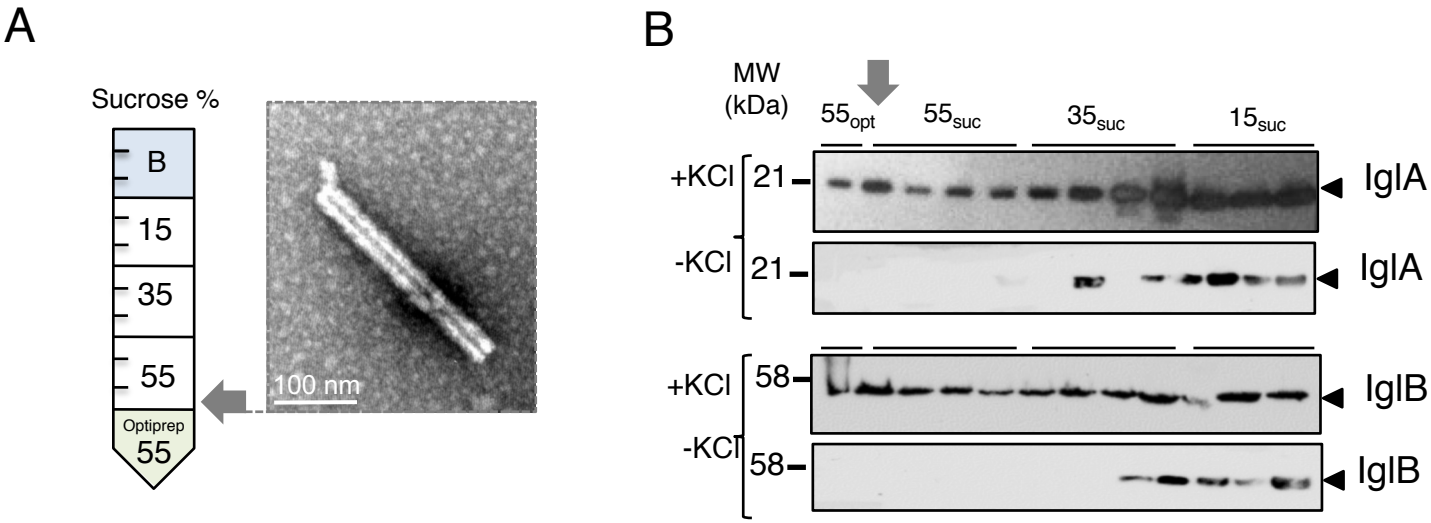

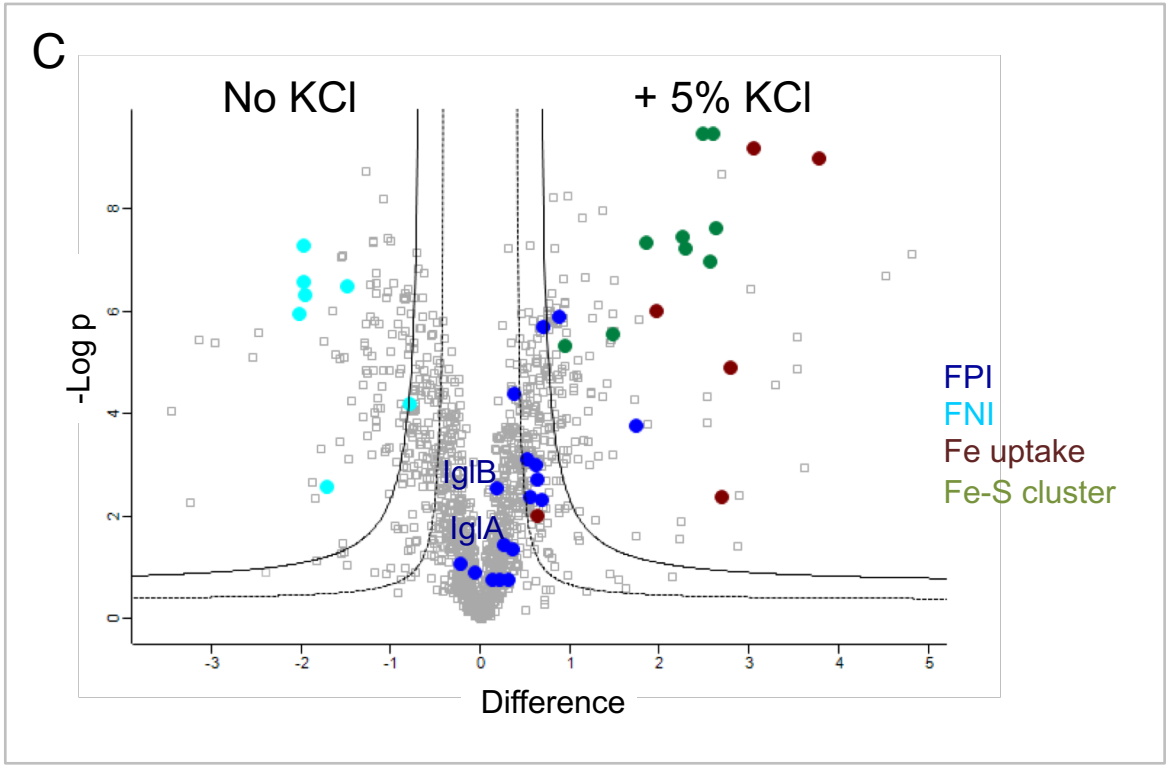

Figure 1. Ziveri et al.

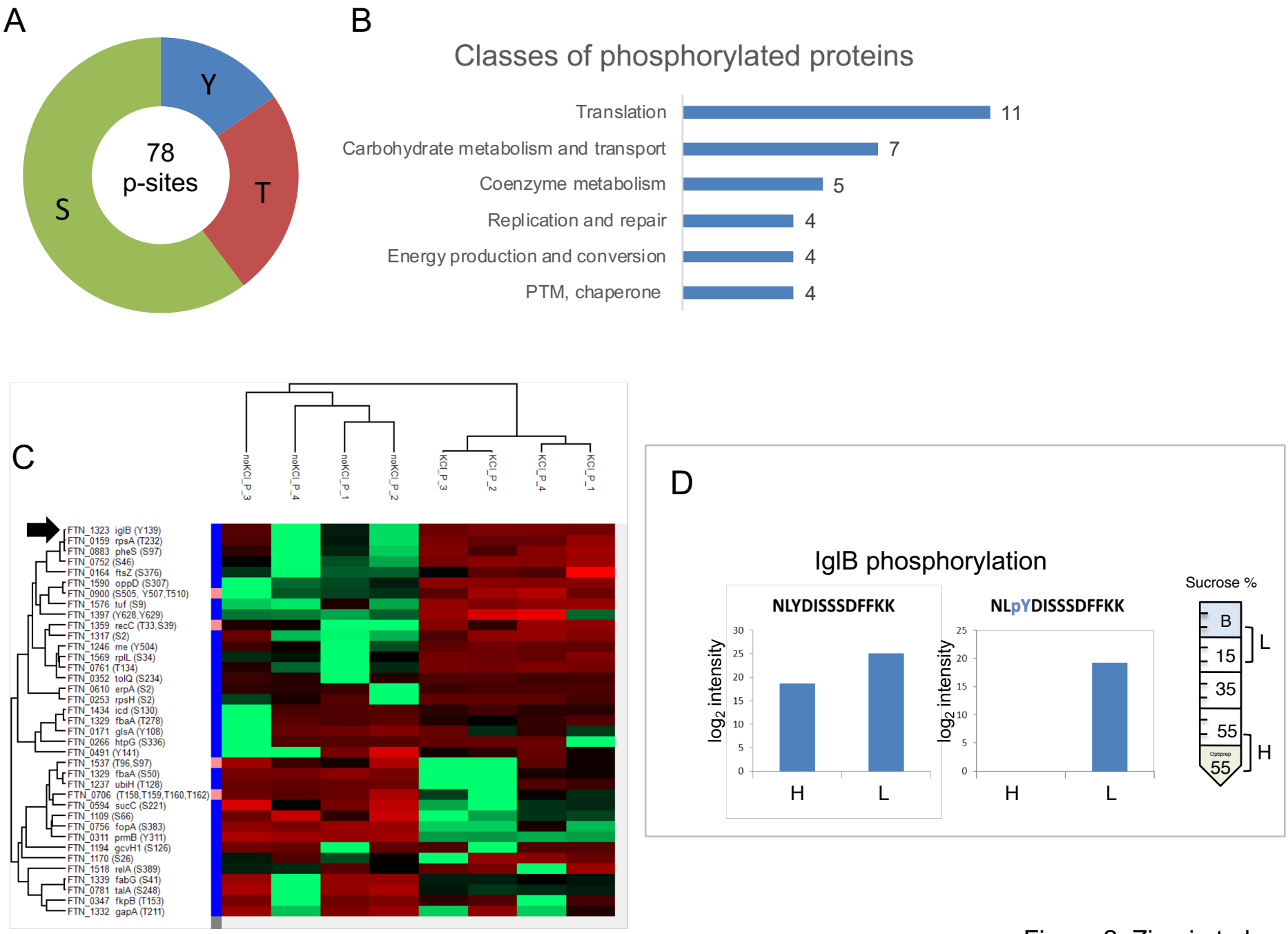

Figure 2. Ziveri et al.

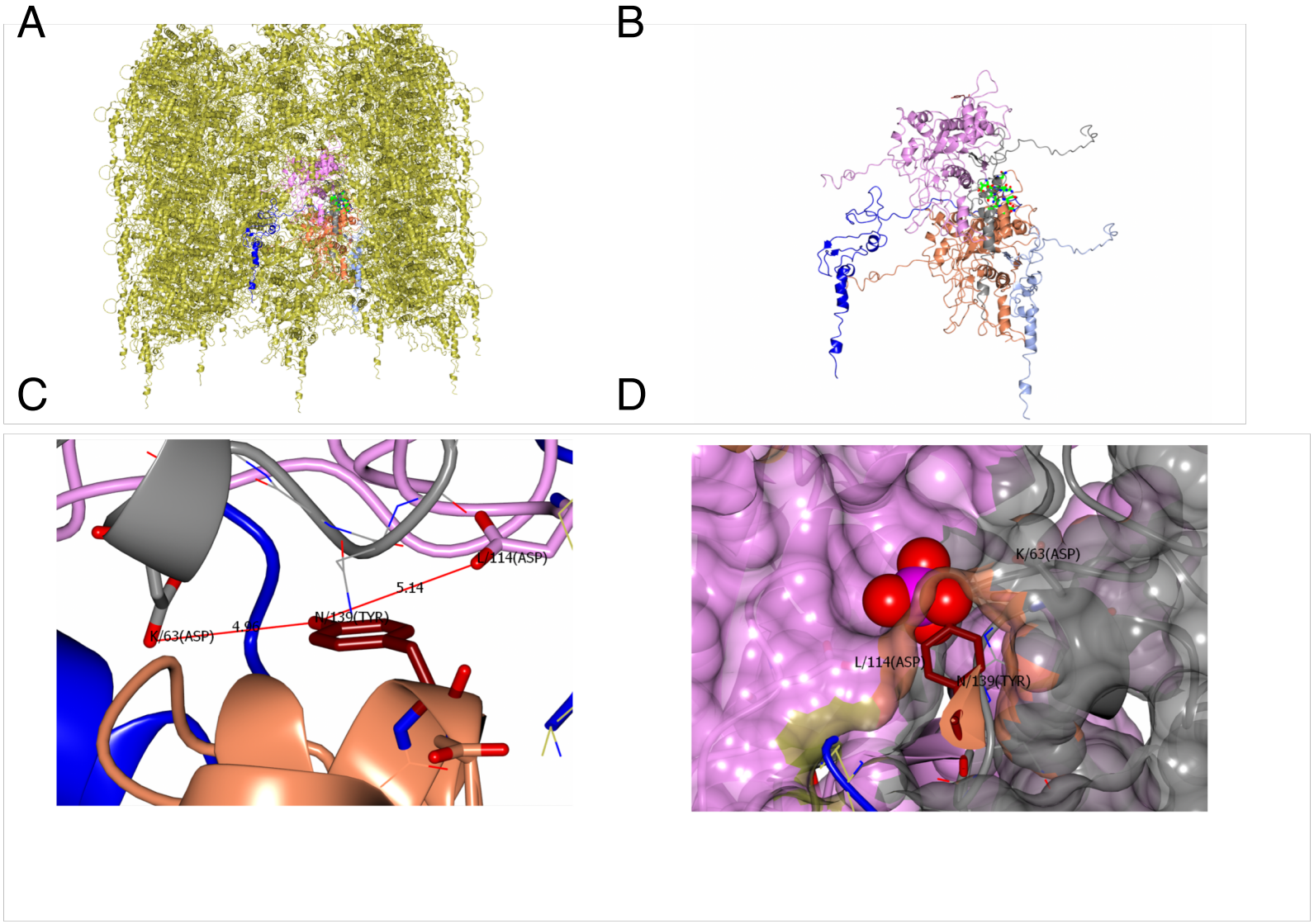

Figure 3. Ziveri et al.

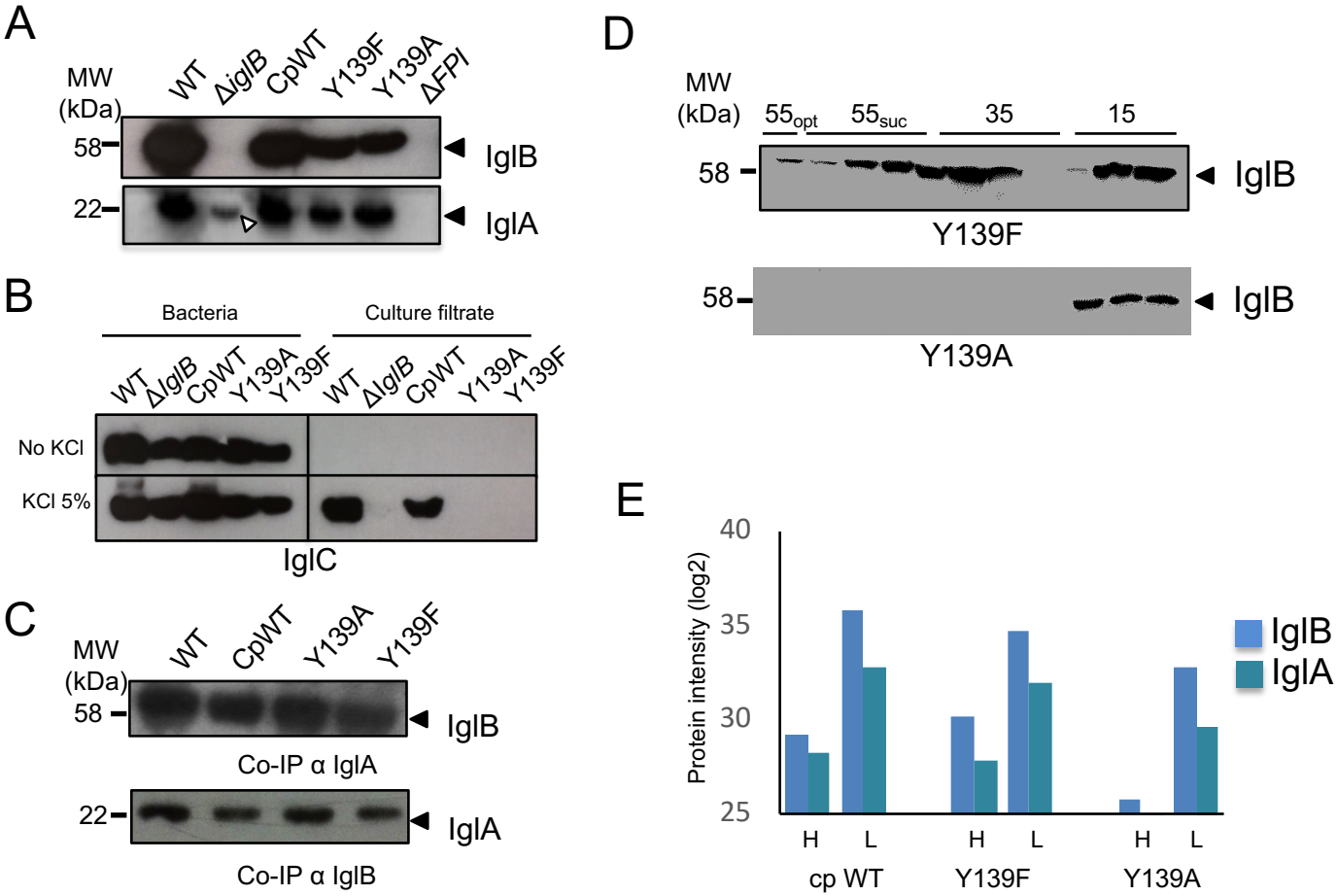

Figure 4. Ziveri et al.

A

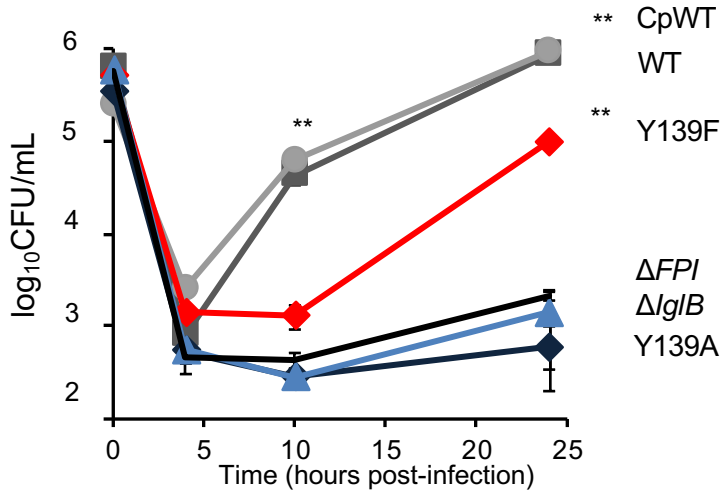

B

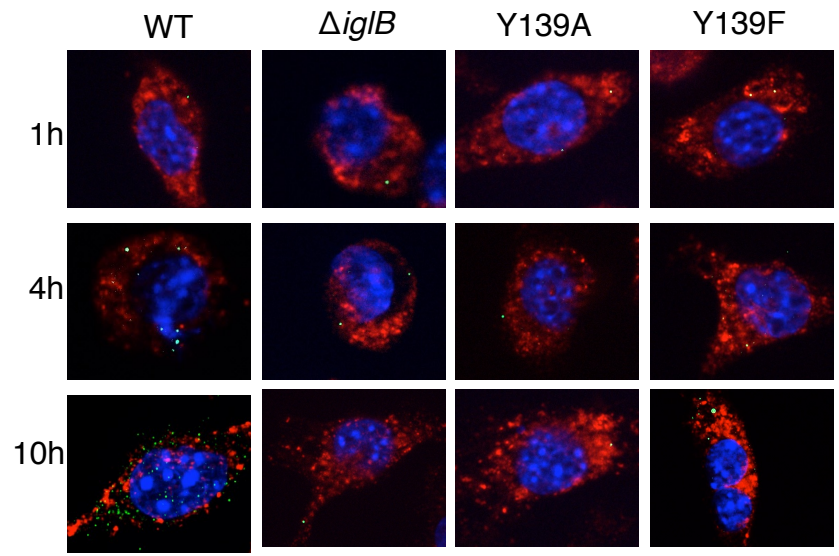

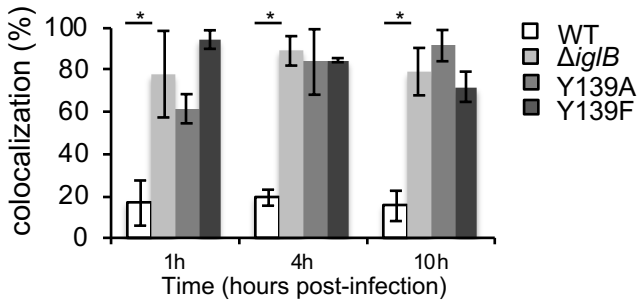

Figure 5. Ziveri et al.

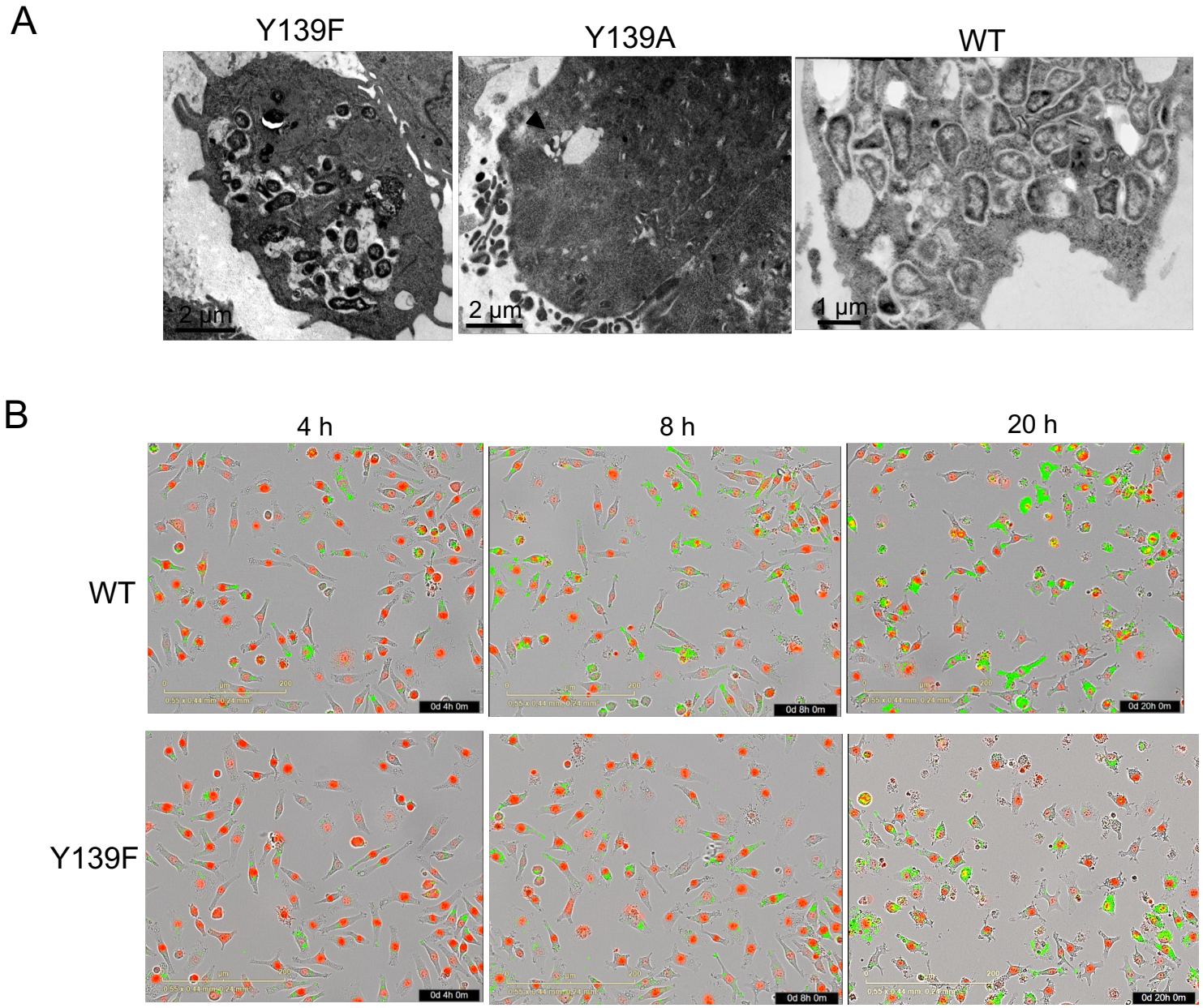

Figure 6. Ziveri et al.

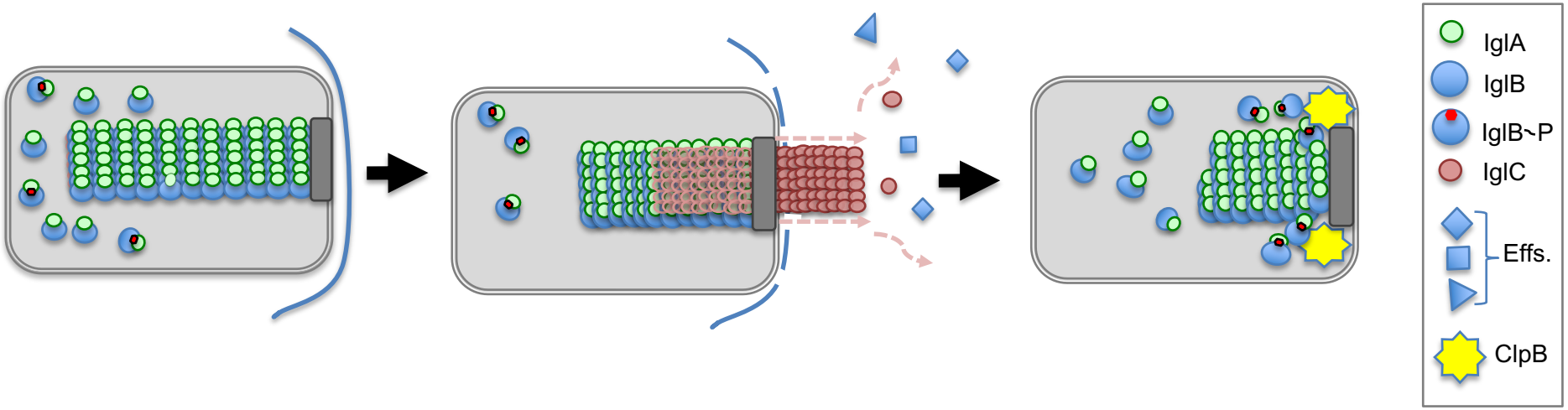

Figure 7. Ziveri et al.